

Valorização de Resíduos de Madeira da Construção Civil: Integração do Processo de Torrefação para a Produção de Biocarvão

Valorization of Construction Wood Waste: Integrating the Torrefaction Process for Biocoal Production

Thais Barbosa

Graduate Program in Mechanical Sciences
Department of Mechanical Engineering

UNIVERSITY OF BRASÍLIA FACULTY OF TECHNOLOGY

### University of Brasília Faculty of Technology Graduate Program in Mechanical Sciences

Valorização de Resíduos de Madeira da Construção Civil: Integração do Processo de Torrefação para a Produção de Biocarvão

Valorization of Construction Wood Waste: Integrating the Torrefaction Process for Biocoal Production

Dissertation submitted as a requirement for obtaining a master's degree in mechanical sciences.

**Author: Thais Barbosa** 

Advisor: Prof. Dr. Edgar Amaral Silveira, ENM/UNB

Brasília-DF, March 27, 2025

### University of Brasília Faculty of Technology Graduate Program in Mechanical Sciences

Valorização de Resíduos de Madeira da Construção Civil: Integração do Processo de Torrefação para a Produção de Biocarvão

Valorization of Construction Wood Waste: Integrating the Torrefaction Process for Biocoal Production

#### THAIS BARBOSA

DISSERTATION SUBMITTED AS A REQUIREMENT FOR THE DEGREE OF MASTER IN MECHANICAL SCIENCES.

#### APPROVED BY:

Prof. Dr. Edgar Amaral Silveira, ENM/UnB (http://lattes.cnpq.br/3018359232062233)

Advisor

Prof. Dr. Ananias Francisco Dias Júnior, DCFM/UFES (http://lattes.cnpq.br/2428652077952117)

External examiner

Prof. Dr. Thiago de Paula Protasio, DCF/UFLA (http://lattes.cnpq.br/3847639263484797)

External examiner

BRASÍLIA-DF, MARCH 27, 2025

FICHA CATALOGRÁFICA

BARBOSA, THAIS

Valorization of Construction Wood Waste: Integrating the Torrefaction Process for Biocoal

Production 2025 xv, 65p., 201x297 mm

Graduate Program in Mechanical Sciences

University of Brasília, Brasília, DF

**BIBLIOGRAPHICAL REFERENCE** 

BARBOSA, THAIS (2025) Valorization of Construction Wood Waste: Integrating the Torrefaction

Process for Biocoal Production. Master's Thesis in Mechanical Sciences, Publication xxx/2025,

Graduate Program in Mechanical Sciences, University of Brasília, Brasília, DF, 65 pages.

ASSIGNMENT OF RIGHTS

**AUTHOR: Thais Barbosa** 

TITLE: Valorization of Construction Wood Waste: Integrating the Torrefaction Process for Biocoal

Production

Degree: Master of Mechanical Sciences

YEAR: 2025

Permission is granted to the University of Brasília to reproduce copies of this thesis and to lend or sell such copies solely for academic and scientific purposes. The author reserves all other publication

rights, and no part of this thesis may be reproduced without the written authorization of the author.

Thais Barbosa

barbosa31thais@gmail.com

### Acknowledgments

First and foremost, I thank God, who was my strength in adversity and my guiding light throughout this journey. To my best friend, Heidy, I am eternally grateful for believing in me, supporting me during challenging moments, and celebrating every achievement. To Mr. Waldemiro (in memoriam) and Olivia, I express my heartfelt gratitude for their patience, kindness, and trust.

To the friends who accompanied me on this journey, with words of encouragement, laughter, and constant support, you made this path lighter and more meaningful—thank you so much. Each act of friendship was an essential source of fuel to reach this goal.

I am deeply grateful to everyone who, in some way, contributed to turning this dream into reality. My advisor, Prof. Dr. Edgar, whose trust and partnership were fundamental during the entire development of this research.

To the team at the Forest Products Laboratory, who supervised all the experiments, I express my sincere appreciation for their availability, patience, expertise, and support. You were an essential part of this achievement, and each advancement reflects a piece of your dedication.

"Quem tudo suporta em silêncio calúnia, agressões, injúrias - conquista uma autoridade moral que faz calar os opositores e transforma aversão em admiração."

Chico Xavier

#### **ABSTRACT**

The construction industry in Brazil plays a vital role in the economy, with growing interest in sustainable alternatives, particularly in waste-to-energy solutions. Construction wood waste (CWW) represents a biomass source with economically valuable applications, such as use as fuel in the energy market. However, one of the main challenges for implementing CWW in urban centers is the continuous availability of materials to meet demand. Additionally, contaminants such as mortar increase the ash content during combustion. High ash content is a key factor contributing to equipment corrosion and slag formation, reducing machinery lifespan and efficiency. In this context, blending different biomass types has emerged as a viable solution to maximize waste utilization and minimize ash content. This study proposes an innovative approach to enhance CWW as a biofuel through torrefaction, using a 50:50 blend of CWW and Eucalyptus sp., torrefied at 200 °C (B200), 250 °C (B250), and 300°C (B300) for 50 minutes. A comprehensive analysis evaluated the performance of the torrefaction process, examining its kinetics and indices, as well as elemental properties, proximate analysis, calorific properties, physical characteristics (bulk density and scanning electron microscopy—SEM), energy density, and combustion behavior, including biofuelrelated emissions. Results indicate that the most efficient treatment was B250, with an ash content of 1.24%, a higher heating value of 20.76 MJ kg<sup>-1</sup>, a solid yield of 86.88%, an energy yield of 91.25%, and a bioenergy density of 6.38 GJ m<sup>-3</sup>. Replacing 1 m<sup>3</sup> of diesel oil, fuel oil, gasoline, or 1 ton of coal with B250 could reduce CO<sub>2</sub>eq. emissions by 590.88 kg, 620.85 kg, 469.68 kg, 770.49 kg, and 1,894.4 kg, respectively. This study aligns with the Sustainable Development Goals (SDGs) 7, 11, 12, and 13, contributing to the development of sustainable cities, responsible waste management, and climate action.

**Keywords**: Waste-to-Energy; Sustainable Construction Waste; Torrefied Biofuel Blends; Bioenergy Performance; CO<sub>2</sub> Emissions Reduction

#### **RESUMO**

A indústria da construção civil no Brasil desempenha um papel fundamental na economia, com interesse crescente em alternativas sustentáveis, particularmente em soluções de conversão de resíduos em energia. Os resíduos de madeira da construção civil (CWW) representam uma fonte de biomassa com aplicações de valor econômico, podendo ser utilizados no mercado como combustível. No entanto, um dos principais desafios para a implementação do CWW em centros urbanos é a disponibilidade contínua de materiais para atender à demanda. Além disso, a presença de contaminantes, como argamassa, eleva o teor de cinzas durante o processo de combustão. Esse alto teor é um dos fatores que contribuem para a corrosão de equipamentos e a formação de escória, reduzindo a vida útil e a eficiência das máquinas. Diante desse cenário, a formação de misturas de diferentes biomassas tem se mostrado uma solução viável para maximizar o aproveitamento desses resíduos e minimizar o teor de cinzas. Este estudo propõe uma abordagem inovadora para melhorar o uso do CWW como biocombustível por meio da torrefação, utilizando uma mistura de 50:50 de CWW e Eucalyptus sp., torrificada a 200 °C (B200), 250 °C (B250) e 300 °C (B300) por 50 minutos. Uma análise abrangente avaliou o desempenho do processo de torrefação (cinética e índices), analisando propriedades elementares, análise química imediata, propriedades caloríficas, físicas (densidade aparente e microscopia eletrônica de varredura - SEM), densidade energética e propriedades energéticas, examinando o comportamento de combustão e as emissões relacionadas ao biocombustível. Os resultados indicam que o tratamento mais eficiente foi o B250, com 1,24% de cinzas, poder calorífico superior de 20,76 MJ kg<sup>-1</sup>, rendimento sólido de 86,88%, rendimento energético de 91,25% e densidade bioenergética de 6,38 GJm<sup>-3</sup>. A substituição de 1 m<sup>3</sup> de óleo diesel, óleo combustível, gasolina ou 1 tonelada de carvão mineral por B250 poderia reduzir as emissões de CO<sub>2</sub> eq em 590,88; 620,85; 469,68; 770,49; e 1894,4 kg, respectivamente. O estudo está alinhado aos Objetivos de Desenvolvimento Sustentável 7, 11, 12 e 13, contribuindo para cidades sustentáveis, gestão responsável de resíduos e ações climáticas.

Palavras-chave: Conversão de resíduos em energia; resíduos sustentáveis da construção; misturas de biocombustíveis torrificados; desempenho bioenergético; redução de emissões de CO<sub>2</sub>

# LIST OF ABBREVIATIONS AND ACRONYMS

## **Index Summary**

## Nomenclature

Nomenciature	
Blend (raw)	В
Blends torrefied at 200° C	B200
Blends torrefied at 250° C	B250
Blends torrefied at 300° C	B300
Construction and demolition waste	CDW
Construction Wood Waste	CWW
Derivative thermogravimetry	DTG
Emission factor	EF
Energy mass-coefficient -index	<b>EMCI</b>
Energy yield	EY
Equivalent volume	EV
Eucalyptus sp.	EUC
Fixed carbon	FC
Fossil fuel	L
Higher heating value	HHV
Hydrogen	H
Lower heating value	LHV
Municipal solid waste	MSW
Reference for liquid fossil fuels	RFF
Refuse-derived fuel	RDF
Solid yield	SY
Specific chemical bioexergy	SCB
Specific torrefaction temperature	TH
Sustainable development goals	SDGs
Thermogravimetric analyzer	TGA
Torrefaction severity factor	TSF
Torrefaction severity index	TSI
Volatile matter	VM
Waste-to-energy	WtE
Weight loss	WL

## Symbols

Absolute difference	$diff^{T}(t)$
Burnout temperature	$T_f$
Burnout time	$t_f$
Reaction temperature	$T_H$
Carbon	$\mathcal{C}$
Carbon dioxide	$CO_2$
Carbon dioxide equivalent	$CO_{2e}$
Carbon monoxide	CO
Coefficient of determination	$R^2$

Ignition index	$D_i$
Ignition temperature	$T_i$
Ignition time	$t_i$
Index of torrefaction	$I_{torr}$
kinetic constants	$k_i$
Nitrogen	N
Oxygen	0
Optimum alpha	$\alpha_{opt}$
Peak temperature	$T_p$
Peak time	$t_p$

# LIST OF FIGURES

Figure 1. A schematic of property variation of biomass undergoing torrefaction (source: Chen et al.
(2015)[3])
Figure 2. Reaction mechanisms occurred during biomass torrefaction. Source: Chen et al. (2021)
[52]28
Figure 3.(a) Thermogravimetric analyses (TGA) and (b) derivative thermogravimetric (DTG)
analyses of the standards of cellulose, hemicellulose, and lignin. (Source: Chen et al. (2015)[3]31
Figure 4. Workflow diagram of the presented investigation and related sustainable development goals
(SDG 7, 11, 12, and 13). Source: Barbosa et al., (2024) [71]
Figure 5. Samples and Analyses (Blend CWW and EUC). (Font: Author)
Figure 6. Ternary diagram of proximate analysis for <i>Eucalyptus</i> , CWW, B, B200, B250 and B300.
(b) Van Krevelen diagram. Data for comparison: Pinus Radiata (P-raw, 250, 280 °C [118]),
Demolition wood residues (DW-raw, 250, 270 and 300 °C [14]), Blend composed of c construction
and demolition wood (DC) and refuse-derived fuel (RDF-raw and 220° C [2]), Pinus elliottii (P-
raw and 300 °C [124]), <i>Eucalyptus</i> sp. (E-raw, 240, 260 and 280 °C [113]. Source: Barbosa et al.,
(2024) [71]
Figure 7.Linear correlation between SY and TSI and proximate analysis ((a) and (d)), ultimate
analysis ((b) and (e)), and calorific analysis ((c) and (f) Source: Barbosa et al., (2024) [71]48
Figure 8. Linear correlation between indexes (I_torr and TSF) and proximate analysis ((a) and (d)),
ultimate analysis ((b) and (e)), and calorific analysis ((c) and (f). Source: Barbosa et al., (2024) [71]
49
Figure 9. Variation of biomass coloration according to the severity of the torrefaction process and
SEM images with 400 and 1000X for (a) raw Eucalyptus sp., (b) CWW, (c) B200, (d) B250, and (e)
B300. Red circles indicated the contamination on CWW Source: Barbosa et al., (2024) [71]50
Figure 10. Experimental SY (%) and treatment temperature (°C) for torrefaction treatments. (b)
Three-dimensional surface and two-dimensional contour mapping for the calculated SY as a function
of treatment time and temperatures. (c) Three-dimensional surface and two-dimensional contour
mapping for TSI as a function of treatment time and the reaction temperatures, highlighting the low,
intermediate, and higher curvatures. White dashed lines indicate the transition from light to severe
torrefaction. (d) Correlation between weight loss (%) and <i>TSFdim</i> for optimum alpha value (3.8).
(e) Profile of the coefficient of determination R <sup>2</sup> . (f) Three-dimensional surface and two-dimensional

contour mapping for <i>TSFdim</i> highlighting the low, intermediate, and higher cur-	vatures. Source:
Barbosa et al., (2024) [71]	52
Figure 11. (a) Comparison between experimental (markers) and numerical (lines) S'	Y. (b) Arrhenius
plot: calculated reaction rates competition for 200-300 °C torrefied blends. Source	: Barbosa et al.,
(2024) [71]	55
Figure 12. Mass loss %, based on dry mass - db (a) and DTG curves at 20 $^{\circ}$ C min-1	(b) B, (c) B200,
(d) B250, and (e) B300 combustion. Source: Barbosa et al., (2024) [71]	56

# LIST OF TABLES

Table 1. Summary of WtE research on wooden construction waste
Table 2. Classification and Destination of Construction Waste
Table 3. Summary of studies on wood composition of construction waste in different Brazilian cities
2
Table 4. Physicochemical transformation and property variations of biomass before and after
torrefaction2
Table 5. Formulation of the four torrefaction severity indexes
Table 6. Energetic and physical characterization of the raw materials blend4
Table 7.Properties of the raw (B) and torrefied blends (B200, B250 and B300). Proximate (volatil
matter (VM), fixed carbon (FC), and ash content in %), ultimate (CHON in %), and calorific (LHV
HHV and SCB in MJ kg-1) analysis. Torrefaction performance index (SY, TSI, TSF, I_torr, EY
EMCI and Bioenergy density)4
Table 8. Kinetic parameters (activation energy and pre-exponential factor) and curve fit quality (R <sup>2</sup> )
5
Table 9. Combustion characteristic parameters of raw feedstock (B) and their torrefied product
(B200, B250 and B300)5
Table 10.Fossil fuel equivalence for 1 m3 of biomass and potential CO2 retention prevented by th
valuation of CWW5

## **SUMMARY**

1 Introduction	15
1.1 Problem Characterization	15
1.2 Applications	17
1.3 Objective	17
1.3.1 General Objective	17
1.3.2 Specific Objectives	17
1.4 Structure of the Work	18
2 Theoretical Foundation	19
2.1 Sustainability and energy transition	19
2.2 Construction Sector	20
2.2.1 Classification of Construction Waste	21
2.2.2 Wood Waste	22
2.3 Biomass	23
2.3.1 Biomass Composition and Structural Characteristics	24
2.3.2 Characterization of Biomass	25
2.3.3 Challenges and Optimization of Biomass for Energy Use	25
2.4 Torrefaction	26
2.5 Biomass Combustion	29
2.5.1 Combustion of Raw vs. Torrefied Biomass	30
2.5.2 Thermogravimetric Analysis	30
3 Material and Methods	32
3.1 Feedstock	33
3.2 Chemical and Physical Characterization	33
3.2.1 Proximate Analysis	33

3.2.2 Ultimate Analysis	34
3.2.3 Calorific Analysis	35
3.2.4 Physical analysis	35
3.3 Torrefaction	36
3.3.1 Torrefaction experiments	36
3.3.2 Torrefaction performance	37
3.3.3 Torrefaction kinetics	39
3.4 Combustion behavior	40
3.4.1 Potential CO <sub>2</sub> retention	41
4 Results and discussions	42
4.1 Chemical Properties and Energetic Parameters	42
4.1.1 Feedstock quality	42
4.1.2 Raw and torrefied blends	43
4.2 Physical change	48
4.3 Torrefaction performance	51
4.3.1 Torrefaction Severity and Indexes	51
4.3.2 Torrefaction kinetics	54
4.4 Combustion behavior	55
4.5 Fossil fuels equivalence and CO <sub>2</sub> emission mitigation	59
5 Limitations and prospects	61
6 Conclusion.	62

#### 1 Introduction

#### 1.1 PROBLEM CHARACTERIZATION

Civil construction is one of Brazil's most critical sectors for developing and strengthening its economy [1]. The wood waste generated in the construction industry is a biomass source with economic value applications and can be used in the market as fuel. Construction wood waste (CWW) contains about 1% to 2% of the weight of non-woody materials [2]. Despite its sustainability, drawbacks hinder biomass as fuel, such as low density and specific heat, high moisture and oxygen content, hygroscopicity, and heterogeneity [3].

Waste-to-energy (WtE) technologies are actively being developed as part of efforts to reduce reliance on coal and natural gas. The WtE can be performed through thermochemical processes such as torrefaction, hydrotreatment, pyrolysis, and gasification [4], [5], [6], [7]. Torrefaction is a thermal treatment process within the 200–300 °C temperature range, lasting for 40–60 minutes, under an inert or oxygen-lean atmosphere [3], [8]. Torrefaction pre-treatment is particularly interesting because it can convert biomass into a coal-like fuel with lower global warming potential, generating a final product of high energy quality and providing benefits in transportation, logistics, and storage [9], [10].

CWW as a solid biofuel is aligned with several United Nations Sustainable Development Goals (SDGs). Specifically, it contributes to SDG 7 by promoting clean, sustainable, and affordable energy conversion and enhancing biomass integration in the energy mix [11]. It is associated with SDG 11 by reducing environmental impact, improving air quality, and creating job opportunities within sustainable cities [11], [12]. By converting CWW into energy, landfills and the environmental impacts of waste disposal can be mitigated, aligning with SDG 12: Responsible Consumption and Production. Adding value to the waste as a biofuel is also related to SDG 13, which emphasizes reducing the use of fossil fuels and actions to combat climate change [11].

One of the bottlenecks for implementing WtE of CWW in large urban centers is the continuous availability of raw materials to meet the energy demand, allied with the CWW contaminations, that promotes high ash content. In this sense, a viable solution would be the combination of different biomass sources to compose a mixture capable of providing a constant volume of supplies [13]. Previous literature has contributed to the torrefaction field by exploring the pre-treatment of CWW and other lignocellulosic biomass (Table 1).

As indicated in Table 1, the literature primarily focused on the influence of torrefaction severity on the resulting torrefied product, alongside its characterization concerning proximate,

calorific, and ultimate analyses. However, a noticeable gap exists in understanding the effects of blending CWW and *Eucalyptus* on ash content reduction, torrefaction kinetic modeling, and combustion behavior.

Table 1. Summary of WtE research on wooden construction waste.

Feedstock	Torrefaction	Analysis	Performance	Application	Ref
DW	Equipment: Small-scale reactor SOLO furnace Temp.: 250–300 °C Residence time: 15 min Heating rate: 10 °C min <sup>-1</sup>	Proximate, Ultimate	-	Energetic characteristics/ Heavy metals (Cd, Pb, and Zn)	[14]
DC: MSW and DC:RDF	Equipment: Bench-scale reactor Temp.: 220 °C Residence time: 90 min	Proximate Ultimate Cl and S HHV	SY and EY	Toxic organic emissions/ Ash and trace metals/ Polychlorinated dibenzo-p-dioxin and dibenzofuran	[2]
DC (a blend of solid wood and panels)	Equipment: Electric furnace Temp.: 280 °C Residence time: 60 min Heating rate: 1.5 °C min <sup>-1</sup>	Proximate HHV, LHV	SY	Energetic characteristics/	[15]
CDW	Equipment: Electric furnace Residence time: 15–45 min	Ash Ultimate Cl and S HHV Bulk density	SY	Microwave power levels / Fuel and thermochemical Properties/ Temperature profile	[16], [17]
CWW and Eucalyptus (50:50)	Equipment: Macro-TG Analyzer Temp.: 200–300 °C Residence time: 50 min Heating rates: 7 °C min <sup>-1</sup>	Proximate Ultimate Bulk density HHV	Kinetics / SY, TSI, TSF, EY, SCB	Direct combustion/ Released volatiles/ Potential CO <sub>2</sub> retention	Study

DW: demolition wood; DC: demolition and construction wood; MSW: municipal solid waste with a 5–20 wt.% food waste content %; RDF: refuse-derived fuel with less than 5 wt.% of food waste; CDW: woody construction demolition waste; HHV: high heating value; LHV: low heating value; EY: energy yield; SY: solid yield; BD: bulk density; ED: energy density.

In this context, this study seeks to explore how blending CWW, a readily available wood residue with high ash content, with *Eucalyptus* biomass—a species known for its energy potential and low ash content—affects the quality of the resulting biofuel. The 50:50 ratio was chosen for operational ease, allowing researchers to replicate the results on an industrial scale. The assumption under investigation suggests that the formation of blends, coupled with torrefaction, holds the potential to emerge as a solution for maximizing the utilization of CWW while simultaneously minimizing ash content.

#### 1.2 APPLICATIONS

Construction wood waste holds considerable potential for sustainable energy applications. The biomass obtained from shredding this waste is commonly employed as a renewable fuel in industrial boilers and furnaces and has demonstrated efficiency in processes such as grain drying and other thermally driven operations.

Further optimization can be achieved through energy densification techniques, which convert the material into high-energy-density formats such as pellets and briquettes. These densified biofuels not only enhance combustion efficiency but also facilitate handling, storage, and transportation.

To maximize the energy recovery from construction wood residues, thermochemical conversion technologies—including torrefaction, combustion, pyrolysis, and gasification—are essential. Among these, torrefaction improves the physicochemical properties of biomass by increasing its calorific value, hydrophobicity, and grindability, making it a more suitable and efficient solid fuel. In contrast, pyrolysis enables the production of high-value products such as bio-oil and biochar. These advanced technologies contribute to greater energy efficiency and reduced greenhouse gas emissions, supporting global sustainability goals and reinforcing circular economy principles.

#### 1.3 OBJECTIVE

#### 1.3.1 General Objective

To investigate the potential of integrating torrefaction as a valorization pathway for construction wood waste (CWW) through the development of a torrefied biofuel blend with enhanced energy performance and reduced ash content.

#### 1.3.2 Specific Objectives

- To formulate and assess a 50:50 blend of CWW and Eucalyptus sp. as a renewable solid biofuel, aiming to mitigate the high ash content associated with contaminated construction residues.
- To thermochemically treat the biomass blend via torrefaction at distinct severity levels (200, 250, and 300 °C) and evaluate its influence on energy densification, ash minimization, and physicochemical enhancement.
- To characterize the torrefied products in terms of proximate and ultimate composition, calorific values, bulk density, and morphological transformations through SEM imaging.

- To model the torrefaction kinetics using a two-step consecutive reaction approach, quantifying key kinetic parameters such as activation energy and pre-exponential factors.
- To evaluate combustion behavior under controlled thermal conditions, identifying ignition, peak, and burnout parameters, and calculating combustion performance indices.
- To estimate bioenergy performance indices, including energy yield, energy mass-coefficient index (EMCI), specific chemical bioexergy (SCB), and torrefaction severity indicators.
- To quantify the potential reduction in CO<sub>2</sub> equivalent (CO<sub>2</sub>eq) emissions through fossil fuel substitution and to determine the theoretical carbon retention potential per energy unit of the torrefied blend.

#### 1.4 STRUCTURE OF THE WORK

In Chapter 2, a literature review is presented on the study topic, addressing the main concepts related to lignocellulosic waste, construction and demolition waste, thermochemical conversion pathways, torrefaction kinetics, and combustion behavior. Chapter 3 then describes the methodology developed to obtain the results. The experimental results and their analyses are discussed in Chapter 4. Finally, the conclusions are presented in Chapter 5.

#### 2 THEORETICAL FOUNDATION

The valorization of wood waste as an alternative for energy generation must consider the challenges of sustainability and energy transition. The reuse of construction aggregate materials produced through recycling—can help reduce the consumption of new raw materials, such as timber products, minimizing waste and strengthening the circular economy. Among the techniques used to harness these residues, torrefaction stands out, a thermal process aimed at improving the energy properties of biomass, transforming it into a more efficient and viable fuel option. To deepen this approach, essential concepts are analyzed, such as the kinetics of this process, the combustion of the treated material, and its thermal characteristics, enabling a broader understanding of its energy potential.

#### 2.1 SUSTAINABILITY AND ENERGY TRANSITION

The concept of sustainability has taken center stage in global debates, driven by the urgent challenges of climate change caused by human activity [18],[19]. In this context, the need for mitigation, adaptation, innovation, and technology is crucial to reducing negative socio-environmental and economic impacts. International cooperation is essential, as exemplified by the Paris Agreement and the Conferences of the Parties (COP 30), among other initiatives with aligned objectives, to meet the 2030 Agenda and achieve a balance between social, economic, and environmental dimensions [11].

In 2023, Brazil emitted approximately 2.3 billion metric tons of carbon dioxide equivalent (CO<sub>2</sub>eq)—a significant figure highlighting the urgent need for mitigation measures [20]. Land-use change accounted for 46% of these emissions, followed by agriculture at 28%, energy at 18%, and waste and industrial processes, both at 4% [20]. Public policies and legislation, such as Law 14,993/2024 (Future Fuel Law), the National Climate Change Plan, and others aimed at reducing carbon intensity, are being implemented and regulated. These efforts align with international agreements to ensure a just and inclusive energy transition.

Considering the data presented in the 2024 National Energy Balance (BEN), the electricity matrix is predominantly composed of renewable sources, accounting for 89.2%, while the country's energy matrix is supplied by 49.1% renewable energies. This demonstrates the abundance of sustainable resources available in Brazil, such as biomass, hydroelectric, wind, and solar energy [21].

However, there is still considerable dependence on fossil fuels, especially in the transportation and industrial sectors.

Biomass presents a viable and sustainable alternative to petroleum and coal-derived fuels in this scenario. In the energy sector, this renewable source has broad applicability in electricity generation, transportation, biofuel conversion, and various industries such as paper and pulp, steel, and many others [22]. By providing bioenergy, biomass contributes to economic development and can be combined with carbon capture and storage technologies for negative emissions [22].

According to BEN 2024, biomass accounted for 32.6% of the energy matrix, with 16.8% coming from sugarcane derivatives, 8.6% from firewood and charcoal, and 7.2% from other renewables. In the electricity matrix, it corresponds to 8%, divided into 5.1% from sugarcane bagasse, 2.1% from black liquor, and 0.8% from other biomasses [21].

The energy valorization of biomass waste is aligned with Sustainable Development Goals (SDGs) 7, 11, 12, and 13[11]. Using biomass as an energy source has high potential to deteriorate the energy and industrial sectors, reducing the carbon footprint and promoting the sustainable use of resources. In addition to contributing to the generation of clean and affordable energy, its integration into the energy matrix helps reduce environmental impacts and improve air quality. Additionally, it boosts job creation in sustainable cities, encourages responsible consumption and production, reduces dependence on fossil fuels, and combats climate change [11].

#### 2.2 CONSTRUCTION SECTOR

The construction industry is one of the most dynamic and strategic sectors of the Brazilian economy, playing a fundamental role in economic and social development. In 2024, the sector recorded significant growth of 4.1% in the Gross Domestic Product (GDP) during the first three quarters compared to the previous year, driven by public and private investments, as well as increased demand for infrastructure, housing, and commercial buildings [23].

However, the sector faces significant challenges, especially regarding the management of construction and demolition waste (CDW). CDW accounts for between 41% and 70% of the total mass of urban solid waste generated in the country [24]. In 2023, the estimate was 44,5 million tons [25].

#### 2.2.1 Classification of Construction Waste

According to Federal Law No. 12,305/2010, in § 2 of Chapter I, Article 13, item I, subparagraph "h", "construction waste is considered to be those generated in construction activities, renovations, repairs, and demolitions of civil construction works, including those resulting from the preparation and excavation of land for civil works" [26].

Resolution No. 307/2002 of the National Environment Council (CONAMA) regulates the management of construction waste in Brazil, classifying it into classes A, B, C, and D and defining responsibilities for generators, transporters, and recipients (table 2). It requires municipalities and the Federal District to create management plans to promote reuse, recycling, and proper disposal, reducing environmental impacts. Subsequent updates included rules for transfer areas, sorting, and reverse logistics for paint packaging [27].

Table 2. Classification and Destination of Construction Waste

Class	Characteristics	Destination of C&D Waste
A	Reusable or recyclable waste as aggregates, such as ceramic components (bricks, blocks, tiles, coating plates, etc.), mortar, concrete, and precast concrete elements (blocks, pipes, curbstones, etc.).	Must be reused or recycled as aggregates or sent to construction waste landfills, where they should be disposed of in a way that allows future use or recycling.
В	Recyclable waste for other purposes, such as plastics, paper/cardboard, metals, glass, wood, and others.	Must be reused, recycled, or sent to temporary storage areas, where they should be disposed of in a way that allows future use or recycling.
C	Waste for which no economically viable recycling/recovery technologies or applications have been developed, such as gypsum-based products.	Must be stored, transported, and disposed of in compliance with specific technical standards.
D	Hazardous waste from the construction process, such as paints, solvents, oils, and others, or contaminated waste from demolitions, renovations, and repairs of radiology clinics, industrial facilities, and others.	Must be stored, transported, reused, and disposed of in compliance with specific technical standards.

Source: Resolution No. 307 of the National Environmental Council (CONAMA), 2002, p. 6, [27].

Recycling waste into byproducts reinforces the principle that 'in nature, nothing is created, nothing is lost, everything is transformed,' as stated by French chemist Antoine Lavoisier (1743–1794). This idea highlights the importance of turning waste into resources, promoting sustainability and the circular economy, rather than discarding it as worthless material. According to Pashoalin (2017), recycling reduces costs related to raw materials, transportation, and waste disposal, while also easing landfill pressure and benefiting the environment. Additionally, it creates jobs and income,

improves urban environments, and allows for the reuse of materials in social projects and urban maintenance [28].

#### 2.2.2 Wood Waste

Determining the gravimetric composition of construction waste faces challenges due to the absence of systematic annual reports in Brazil, which makes it difficult to obtain precise data on the representativeness of wood in construction sites. It is estimated that this percentage is approximately 13% [24], but it can vary depending on the type of construction, the region, the volume generated, and even the time of year (rainy season) [29].

Wood is one of the oldest materials used in construction due to its availability in nature, high strength, good thermal insulation properties, and wide variety of industrialized products [30], [31]. Table 3 presents the percentages of wood waste based on case studies from different Brazilian cities.

Table 3. Summary of studies on wood composition of construction waste in different Brazilian cities.

City	Evaluation	Phase of construction	Composition (%	Ref
Maceió	Gravimetric composition	-	6.03	[32]
Rio de Janeiro	Gravimetric composition	CDW debris	2.21	[33]
São Paulo	Relative composition (by mass)	Every multi-story residential building construction	10.2	[34]
Recife	Relative composition (by mass)	Structure	16.6	[34]
Londrinaa	Gravimetric composition	Construction site	11	[35]
Lavras	Gravimetric composition	Dumpsters	2.74	[32]
Rio Branco	Relative composition (by mass)	Construction site	19	[36]
São Carlos	Relative composition (by mass)	Dumpsters	7	[35]
Londrina	Volumetric composition	-	8	[35]
Natal	Volumetric composition	-	15	[37]
Cascavel	Volumetric composition	Construction site	37	[38]

CDW - Construction and demolition waste

The contamination of wood waste represents a significant challenge for its reuse, especially when intended for energy applications. Edo et al. (2017) indicate that wood waste can contain 1% to 2% by mass of non-wood materials [2]. In a study on contamination in wood waste from construction, Lopes et al. (2013) identified that this waste has a diverse composition of contaminants. The analysis revealed the presence of 29% mortar, 30% metal pins (nails), 13% paints, 9% moisture and biological agents, 7% soil, 5% release agent, 3% gypsum, and 4% other materials [39].

Studies investigate the reuse of construction wood waste, highlighting its potential for energy and sustainable purposes. Joyce Sholl et al. (2020) analyze waste management, emphasizing the importance of recycling and reuse [24]. The study promotes sustainable practices in the sector, such as the reuse of materials and the implementation of recycling plants [24]. Monzerrath and Roger (2020) investigate the transformation of wood scraps into biomass pellets, evaluating their feasibility as a source of renewable bioenergy, despite challenges such as high ash content [40].

Gunita et al. (2024) analyze the circularity of wood waste in Latvia, identifying opportunities and challenges to reduce greenhouse gas emissions, emphasizing the importance of government support and Life Cycle Assessment (LCA) in the sustainable management of this waste [41]. Lais (2020) proposes a sustainable management model for construction waste in Limeira, São Paulo, using LCA to minimize environmental impacts and optimize recycling [42]. C.S. Poon et al. (2001) address the separation of materials at the construction site, comparing sorting methods and highlighting the effectiveness of source separation to improve waste management and reduce landfill shortages [43].

Cavalcanti and Alves (2018) suggest transforming wood waste into pellets and briquettes, providing a solution for bioenergy and promoting sustainable practices in the construction sector [44]. Edo et al. (2017) explore the use of torrefaction as a pre-treatment for demolition wood waste to reduce pollutant emissions during energy conversion [2]. The research suggests that torrefaction, combined with air pollution control technologies, can mitigate the environmental impact of lignocellulosic waste.

#### 2.3 BIOMASS

Biomass is an abundant renewable energy source in Brazil, originating from various sources such as forest plantations, agricultural and agro-industrial waste, sewage, wood, and urban solid waste [45]. This diversity gives biomass high energy potential, making it a key component in the transition to a more sustainable energy matrix.

#### 2.3.1 Biomass Composition and Structural Characteristics

Biomass is primarily composed of cellulose, hemicellulose, and lignin, along with small proportions of organic extractives and inorganic minerals. These organic and inorganic components directly influence energy performance and conversion efficiency into biofuels[3], [46], [47], [48]. The mass fractions of these constituents vary depending on the biomass species, and understanding their properties is crucial, as each component exhibits distinct behavior during thermal decomposition [3].

#### **2.3.1.1** Cellulose

Cellulose constitutes approximately 40–60% of biomass (dry basis) [46], [47], [48]. It is a biopolymer composed of a long chain of glucose molecules and can establish intra- and intermolecular hydrogen bonds. The main function of cellulose is related to plant structure [49]. The thermal decomposition of cellulose occurs within the temperature range of 315–400°C [3].

#### 2.3.1.2 Hemicelluloses

Hemicellulose accounts for 15–30% of biomass and is a chemically heterogeneous polysaccharide composed of pentoses and hexoses [46], [47], [48], [49]. Compared to cellulose, hemicellulose has lower degrees of polymerization and undergoes significant thermal degradation, which affects mass yield during the torrefaction process [50]. It decomposes at lower temperatures, ranging from 220 to 315°C, indicating its lower thermal stability [3].

#### 2.3.1.3 Lignin

Lignin represents 10–25% of biomass and is a complex three-dimensional polymer with a high carbon content, which is directly related to its energy content [46], [47], [48], [49]. The thermal decomposition of lignin occurs over a broad temperature range, from 160°C to 900°C [3]. Due to the absence of a distinct degradation peak, lignin remains relatively unaltered during the torrefaction process. As a result, biomass with higher lignin content tends to yield more solid residues [50].

#### 2.3.1.4 Inorganic Minerals and Organic Extractives

Inorganic minerals (ash) typically represent less than 1% of the total wood content [3] while organic extractives range from 3% to 5%, depending on the biomass species analyzed [51].

#### 2.3.2 Characterization of Biomass

Properties characterization is essential for selecting the conversion technology to ensure better efficiency [48].

#### 2.3.2.1 Proximate and Ultimate Analysis

- Proximate analysis evaluates ash content, volatile matter, and fixed carbon, which are fundamental for the combustion profile [49]
- Ultimate analysis determines the proportions of carbon, hydrogen, nitrogen, and oxygen, with carbon being the primary contributor to energy generation during combustion.

#### 2.3.2.2 Ultimate Composition and Heating Value

The composition of biomass shows higher rates of hydrogen and oxygen, and lower rates of carbon compared to fossil fuels. While carbon and hydrogen are sources of heat for combustion, the presence of oxygen reduces the heating value of biomass, favoring CO<sub>2</sub> formation [3]. This relationship is quantified by the atomic ratios O/C (0.4–0.8) and H/C (1.2–2.0) in raw biomass, indicative of its thermochemical reactivity [3], [50]. After torrefaction, carbon retention occurs while oxygen and hydrogen are reduced, resulting in lower O/C and H/C ratios (0.1–0.7 and 0.7–1.6, respectively). This process enhances the energy quality of biomass, increasing its heating value [3].

#### 2.3.3 Challenges and Optimization of Biomass for Energy Use

#### 2.3.3.1 Logistical and Energy Density Limitations

The low density of biomass imposes logistical challenges, such as high storage and transportation costs, while reducing its energy density [50]. Pre-compaction can mitigate these problems by optimizing the net yield of the process [49].

#### 2.3.3.2 Impact of Ash and Oxygen Content

The heating value is inversely influenced by ash and oxygen content. High levels of oxygen promote partial oxidation, releasing less energy, while ash acts as inert material, reducing combustion efficiency [3], [47], [49].

#### 2.3.3.3 THERMOCHEMICAL Conversion Technologies

Although biomass is a sustainable alternative, its direct energy application is limited by characteristics such as hygroscopicity, high moisture content, and low heating value [3]. Thermochemical processes—such as torrefaction, pyrolysis, and gasification—optimize its properties, increasing the heating value and adapting it for biofuel production [45]. These technologies not only reduce dependency on fossil sources [52] but also boost decarbonization efforts, aligning with Brazilian goals for energy transition and combating climate change.

#### 2.4 TORREFACTION

Torrefaction is a thermochemical process in which biomass is subjected to a constant temperature for a predefined time. The thermal treatment occurs in an inert atmosphere, with partial or total absence of oxidizing agents, within a temperature range of 200 to 300°C and a residence time of 40 to 60 minutes [3], [8]. This process induces chemical reactions that transform the physical and chemical properties of the biomass, altering its stability, composition, and energy value [5], [53]. Thus, it becomes a fundamental step to optimize the efficiency and feasibility of energy and industrial applications.

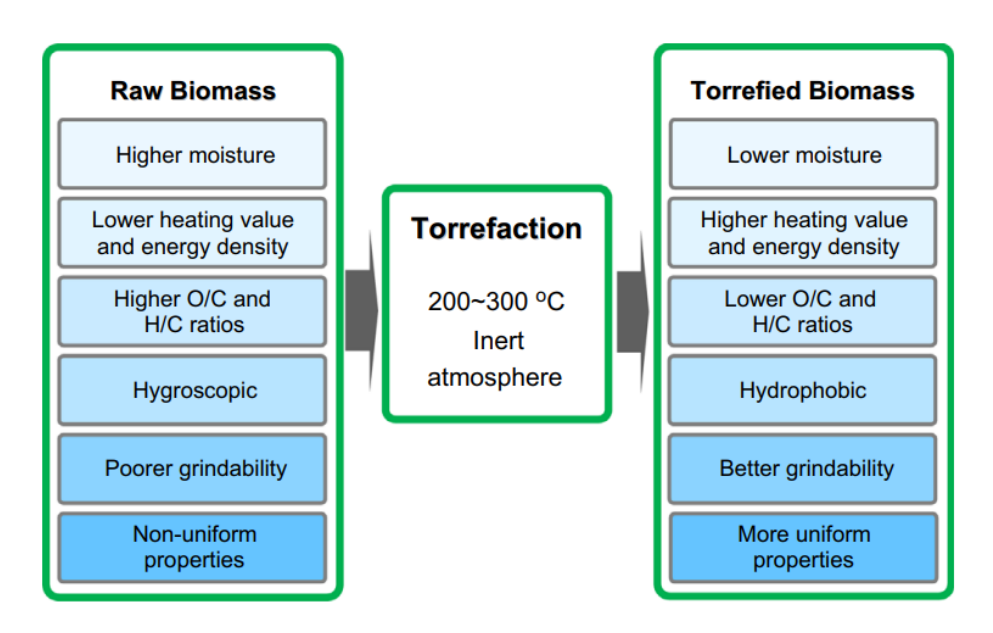


Figure 1. A schematic of property variation of biomass undergoing torrefaction (source: Chen et al. (2015)[3])

The primary objective of torrefaction is to enhance biomass properties for solid biofuel production, aiming to partially or completely replace mineral coal [52]. According to Chen et al. (2015), this process overcomes the limitations of raw biomass for energy applications by modifying

its physicochemical properties, as illustrated in Figure 1 showing biomass characteristics before and after torrefaction [3]. As a result, torrefaction stabilizes biomass and makes it more suitable for subsequent thermochemical processes, such as pyrolysis, gasification, and combustion, functioning as a pre-treatment that enhances the efficiency of these processes [52], [54].

During the torrefaction process, exothermic behavior can be observed during the thermal degradation of hemicellulose and lignin, whereas endothermicity occurs during cellulose degradation [55]. According to Ball et al. (2024, apud Yang et al., 2007) the carbonization process (char formation) is highly exothermic, while volatilization (gas release) is endothermic [56]. Since hemicellulose and lignin produce more solid residue, the exothermic peaks may be attributed to char formation. In contrast, cellulose undergoes rapid devolatilization, resulting in minimal solid residue [56]. Furthermore, as torrefaction severity increases, decarboxylation, dehydration, and demethylation reactions take place, lowering the H/C and O/C ratios and enhancing the material's degree of carbonization and structural stability [52].

Kinetic analysis of torrefaction is essential for process modeling, enabling the prediction of its behavior under various operating conditions and optimization of biomass energy conversion efficiency. These phenomena can be evaluated using kinetic models, which are mathematically represented by Arrhenius equations, describing the thermal degradation rate of biomass constituents as a function of temperature and residence time. Through these models, key kinetic parameters—such as activation energy and conversion rate—can be determined, allowing for necessary adjustments to enhance torrefaction as a biomass valorization technique for energy applications [57], [58], [59], [60], [61], [62].

This process involves three main reactions—decomposition, devolatilization, and depolymerization—and can be divided into four stages: drying, post-drying, torrefaction, and cooling [50]. Devolatilization is defined as the removal of oxygen and volatiles from the sample, occurring at temperatures above 200°C [50]. This phenomenon can be measured by the mass loss rate during thermal degradation, which increases as the temperature rises. The other two reactions, decomposition and depolymerization, involve the conversion of macromolecules in the sample into micromonomers, which are then transformed into condensable and non-condensable volatile gases [50].

The first three stages of torrefaction are classified according to their temperature ranges. The first stage is drying, a non-reactive process that occurs between 50°C and 150°C and requires the highest energy input due to the removal of surface moisture from the sample. The next stage is post-

drying, considered a reactive process, which releases internal moisture and light hydrocarbons within a temperature range of 150°C to 200°C. Only above 200°C does actual torrefaction begin, along with devolatilization [50]. Finally, the cooling stage continues until the sample reaches room temperature.

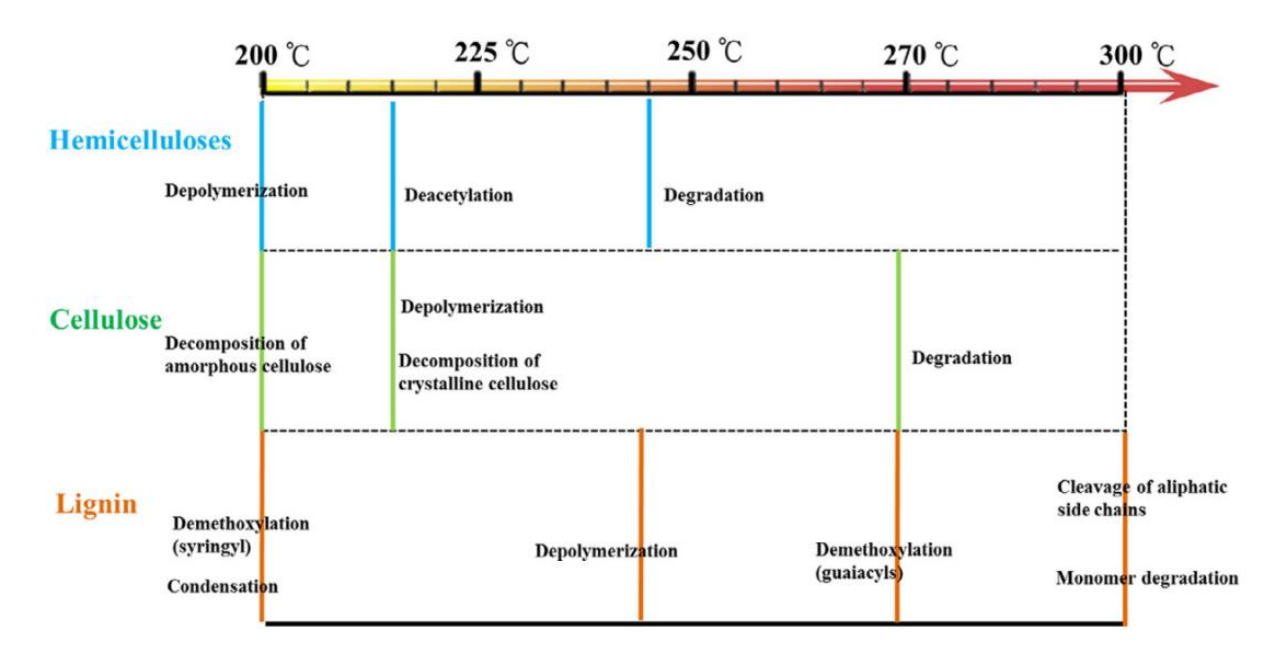


Figure 2. Reaction mechanisms occurred during biomass torrefaction. Source: Chen et al. (2021) [52].

Another important stage is devolatilization, which begins during heating, continues throughout torrefaction, and persists even after the biomass cools down [50], [63]. This process involves the release of volatile compounds, contributing to the chemical and physical transformation of the material, making it more stable and energy dense. Torrefaction occurs at a constant temperature with a defined residence time, classified as light (200-235°C), moderate (235-275°C), and severe (275-300°C)[53].

Thermal degradation of biomass occurs differently for each of its main constituents - namely hemicellulose, cellulose, and lignin. As demonstrated by Chen et al. (2021) and illustrated in Figure 2, the main thermal events occurring during the torrefaction process show that lignin exhibits greater thermal stability compared to cellulose and hemicellulose [52].

Therefore, Table 4 presents the main benefits of this process, highlighting that it contributes to increasing energy density and hydrophobicity. It improves biomass quality, making its storage and transportation simpler and more efficient [50], [52].

Table 4. Physicochemical transformation and property variations of biomass before and after torrefaction

Raw biomass	Physicochemical transformations	Torrefied biomass property
High moisture content	Dehydration	Water bound to molecules is removed by evaporation due to increased temperature, reducing the material's moisture content.
Hygroscopic	Dehydration, Dehydroxylation, Decomposition of amorphous cellulose, Apolar tar in pores	The removal of hydroxyl (-OH) and other polar groups decreases the biomass's affinity for water, making it hydrophobic.
Higher O/C and H/C ratio	Less extent decarbonization, Dehydrogenation, Deoxygenation, Deacetylation, Demethoxylation	The elimination of volatile compounds rich in oxygen and hydrogen concentrates carbon in the material, reducing the O/C and H/C ratios.
Increase in Lower heating value	Devolatilization, Dehydration, Carbonization, Dehydrogenation, Deoxygenation	The reduction of oxygen and hydrogen content relative to carbon increases the material's energy density, raising its heating value.
Improvement in grindability	Hemicellulose decomposition	Hemicelluloses, which are thermally unstable, decompose, making the biomass structure more fragile and facilitating the grinding process.
Reduction in biodegradation	Hemicelluloses decomposition, Lignin modification	Lignin becomes less reactive due to structural changes, and the removal of volatile compounds reduces the material's attractiveness to decomposing microorganisms.

Source: Adapted from Chen et al. (2021) [52]

#### 2.5 BIOMASS COMBUSTION

Combustion is an exothermic reaction where the chemical energy of the fuel is transformed into thermal energy by breaking its molecular bonds. It is a reaction where the fuel reacts with oxygen, releasing energy in the form of heat. During the process, the oxidation of biomass components, such as cellulose, hemicellulose, and lignin, occurs, resulting in the release of carbon dioxide (CO<sub>2</sub>), water vapor (H<sub>2</sub>O), and other byproducts [64]. The efficiency of combustion depends on factors such as moisture content, ignition temperature, and oxygen availability. When performed in a controlled and efficient manner, it is a renewable alternative that contributes to the mitigation of greenhouse gas emissions.

#### 2.5.1 Combustion of Raw vs. Torrefied Biomass

The combustion of raw biomass is a widely used process, especially in small-scale applications, such as firewood for domestic stoves and ovens, among others. During combustion, extrinsic moisture is eliminated, consuming part of the released energy and reducing the thermal efficiency of the process. Consequently, it tends to release more volatiles during combustion, which can lead to the formation of soot and pollutant emissions, such as carbon monoxide (CO) and particulate matter [47]. On the other hand, the combustion of torrefied biomass offers significant advantages compared to raw biomass, releasing fewer volatiles and resulting in cleaner and more efficient combustion [47].

#### 2.5.2 Thermogravimetric Analysis

Combustion profiles, represented by thermograms, are crucial tools for understanding and analyzing fuel combustibility and their application in combustion systems. Thermogravimetric analysis (TG) and its derivative (DTG) are essential tools for understanding and optimizing biomass combustion. These techniques allow for the evaluation of the thermal decomposition of organic components present in biomass (Figure 3, Chen et al. (2015)), identifying different combustion stages: drying, oxidative pyrolysis, and biofuel combustion. The TG curve shows mass losses corresponding to moisture removal, degradation of organic matter, and formation of carbonaceous residues [3]. The DTG curve, obtained from the derivative of TG, highlights the degradation peaks of the main components, allowing differentiation of the thermal stages of biomass.

Combustion parameters, such as ignition temperature, peak temperature, burnout temperature (total combustion temperature), and burn time, are crucial for analyzing combustion performance[65], [66]. Burn time, representing the interval between the onset of mass loss of the dry biofuel and the stabilization of weight, corresponds to the final stage of the combustion process, characterized by the absence of significant mass losses, indicating the complete conversion of the fuel material [66], [67].

Ignition temperature corresponds to the temperature at which there is an abrupt drop in the thermal degradation rate of the sample, signaling the start of combustion [66]. Lower values of this parameter indicate higher reactivity of the biomass, facilitating combustion [65], [67]. Peak temperature represents the point of maximum thermal decomposition rate of the sample, correlating with the volatilization of organic components and the formation of carbonaceous residues [66], [68].

Higher values may indicate the presence of refractory materials or residues not completely oxidized, requiring longer residence times and higher temperatures for complete combustion [65].

During heating, hemicellulose is the first to decompose, usually in the range of 220–280°C, as indicated by the first significant drop in the TG curve and a corresponding peak in the DTG curve [69], [70]. Cellulose, being more resistant, begins to degrade at a higher temperature range of 240–350°C, marked by another drop in the TG curve and a new peak in the DTG curve [69], [70]. Lastly, lignin decomposes more slowly and continuously, ranging between 250–500°C, generating a more gradual TG curve with less defined peaks in the DTG curve [69], [70].

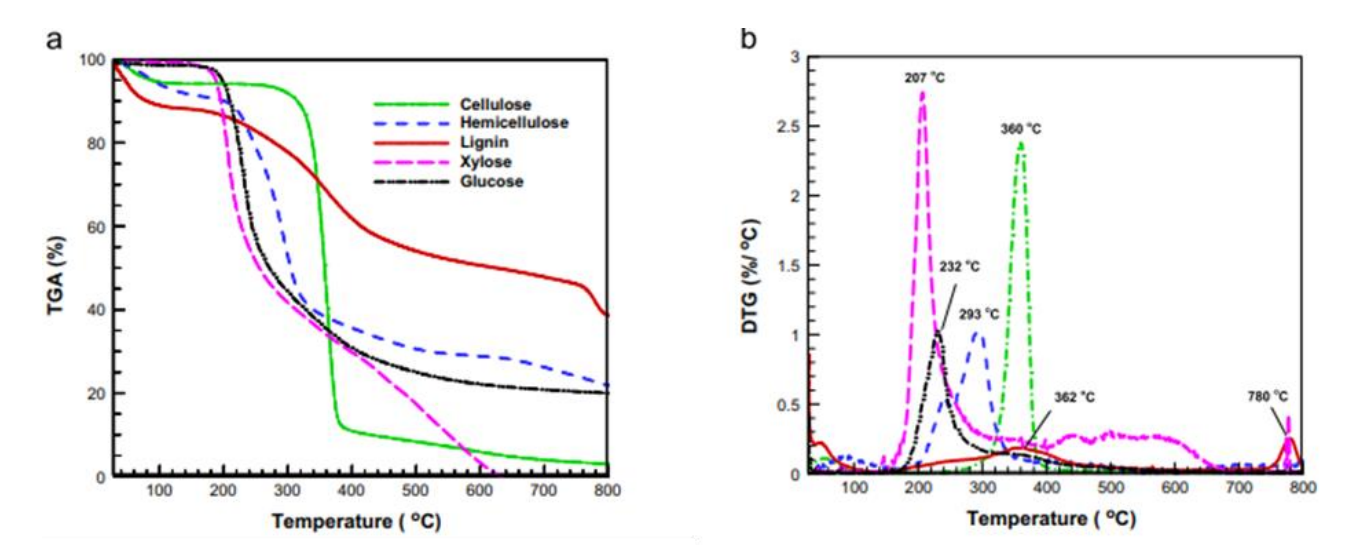


Figure 3.(a) Thermogravimetric analyses (TGA) and (b) derivative thermogravimetric (DTG) analyses of the standards of cellulose, hemicellulose, and lignin. (Source: Chen et al. (2015)[3]

.

#### 3 MATERIAL AND METHODS

This chapter provides a detailed description of the materials and methods used, including the procedures for sample preparation, chemical and physical characterization analyses, torrefaction tests, and the evaluation of the combustion behavior of the blend. The experimental steps were carried out at the Forest Products Laboratory (LPF) of the Brazilian Forest Service, located in Brasília/DF, following standardized protocols to ensure the accuracy and reproducibility of the results. The workflow and the Sustainable Development Goals (SDGs) related to this study are presented in Figure 4.

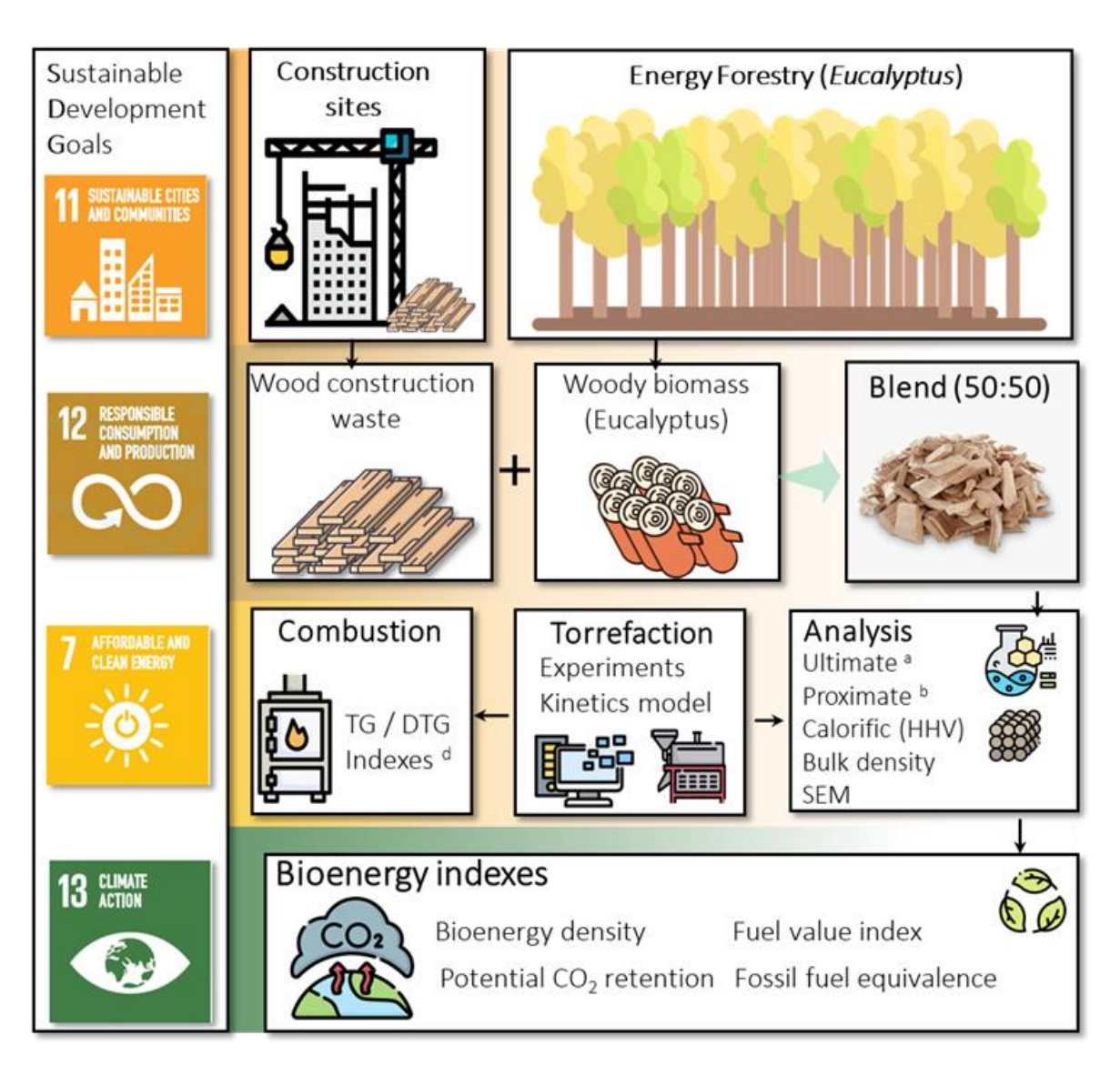


Figure 4. Workflow diagram of the presented investigation and related sustainable development goals (SDG 7, 11, 12, and 13). Source: Barbosa et al., (2024) [71]

#### 3.1 FEEDSTOCK

The experiments were conducted using wood waste from the construction industry, specifically *Pine* sp. boards contaminated with non-wood materials such as mortar and nails (Figure 5). This waste was provided by Tejo Engenharia, located in Brasília-DF, Brazil, for analysis and investigation. For the blend composition, the Brazilian Forest Service supplied samples of *Eucalyptus* sp.[72], [73].

Initially, all nails were removed from the *Pine* sp. boards to prevent damage to the equipment used in laboratory-scale tests. After this step, the boards were cut into pieces up to 5 cm wide and then ground in a hammer mill The ground material was stored in plastic bags to prevent moisture absorption and ensure the integrity of the samples [72], [73].

To ensure the homogeneity of the wood sample from construction waste (construction wood waste, CWW), the material was collected from different points of the packaging, including the lower, central, and upper sections, ensuring that contaminants such as mortar were present in the samples for analysis. The material was then processed in a Willey-type knife mill and sieved using a 60 mesh (0.25 mm) screen, according to ISO 18123:2015, to select the fraction with the appropriate particle size for the experiments [72], [73].

The *Eucalyptus* sp. Sample provided in chip form underwent the same preparation procedures. The material was processed in a Willey-type knife mill and then sieved to select the fraction retained on the 60 mesh (0.25 mm) screen. Before being subjected to experiments and analyses, both the *Pine* sp. and *Eucalyptus* sp. samples, as well as their respective mixtures, were dried in an oven at  $105 \pm 2$  °C to remove residual moisture, ensuring the standardization of the sample content. [72], [73].

#### 3.2 CHEMICAL AND PHYSICAL CHARACTERIZATION

#### 3.2.1 Proximate Analysis

#### Volatile matter content

The volatile matter content (VM) was measured on a dry basis according to ISO 18123 (2015). The analyses were performed in duplicates for *Eucalyptus* sp. chips and triplicates for CWW wood. Samples of approximately 1g were dried to remove all extrinsic moisture in an oven at  $103^{\circ}\text{C} \pm 2^{\circ}\text{C}$  for 2 hours. The material was then removed from the oven and placed in a dedicator for about 15 minutes to cool. Once cooled, the masses of the porcelain crucibles and the samples were measured. With the crucibles covered, the biomass was placed in a muffle furnace at 900°C for 7 minutes (Figure 5). After this procedure, the samples were removed and placed in a desiccator for about 30 minutes

to cool, and finally, the final mass of each sample (crucible mass + sample mass) was measured. Calculation of volatile matter content (VM) by mass difference, according to equation (1):

$$VM = \frac{M_2 - M_3}{M_1} \times 100\% \tag{1}$$

Where VM is the volatile matter content (%),  $M_1$  is the dry mass of the sample,  $M_2$  is the mass of the crucible + dry mass of the sample, and  $M_3$  is the mass of the crucible after the muffle furnace at 900°C.

#### **Determination of Ash Content**

The determination of ash content presented in Figure 5 was performed using a thermogravimetric analyzer (Macro-TG Analyser TGA-2000-A) through complete combustion of the biomass, following ISO 18122 (2015). The analyses were conducted in triplicate with samples of approximately 0.9 g. The percentage of ash content was based on the average of the three samples (Figure 5).

#### Calculation of fixed carbon content

The percentage of fixed carbon (FC) can be determined from the values of volatile matter content (VM) and ash content, as can be seen in the equation (2).

$$FC = 100 - (ash + VM) \tag{2}$$

#### Fuel ratio

This index provides a measure of fuel quality, considering the ratio between fixed carbon, which contributes to heating value, and volatile matter, which is released during combustion. The fuel ratio (FR) was determined by the relationship between fixed carbon (FC) and volatile matter (VM), using equation 3:

$$FR = \frac{FC}{VM} \tag{3}$$

#### 3.2.2 Ultimate Analysis

Ultimate analysis was conducted to determine the proportions of carbon (C), hydrogen (H), and nitrogen (N) in the samples. The wood residue samples were analyzed using a Perkin Elmer 2400 Series II elemental analyzer at the Analytical Center of the University of São Paulo (USP), following

ASTM E777/2008 and ASTM E778/2008 standards. The oxygen (O) content was obtained by difference between the percentages of the biochar components (equation 4).

$$0 = 100 - C - N - H - ash \tag{4}$$

#### 3.2.3 Calorific Analysis

#### Higher heating value (HHV)

The higher heating value (HHV) tests were conducted in triplicate using a PARR model 6400 – Automatic Isoperibol Calorimeter, according to the methodology described by ISO 18125:2017. Pellets (Figure 5) with  $\pm$  1g were prepared for this test. The HHV was determined by the average of two valid tests, calculated in Megajoules per kilogram (MJ/Kg).

#### Lower Heating Value (LHV)

The Lower Heating Value (LHV) was calculated using Equation (5A) [74], which accounts for the hydrogen content (H%) and the latent heat of water vaporization (approximately 600 kcal/kg):

$$LHV = HHV - 600 \times \left(\frac{9H}{100}\right) \tag{5A}$$

Since the Higher Heating Value (HHV) is given in MJ/kg, and considering that 1 kcal = 0.004184 MJ, the LHV is obtained using Equation (5B):

LHV = HHV - 2.5104 × 
$$\left(\frac{9H}{100}\right)$$
 (5B)

#### 3.2.4 Physical analysis

#### Bulk density

The bulk density on a dry basis (0% moisture content) was measured according to ISO 17828:2015, with adaptation for a container with a volume of 16.31 mL. Samples with a particle size of 60 mesh (0.25 mm) had their bulk density calculated as the ratio of mass in grams to the volume of the container in cm<sup>3</sup>. The energy density was obtained by multiplying the HHV by the bulk density.

#### Scanning electron microscopy (SEM)

Scanning electron microscopy (SEM) was performed using a TM-4000Plus instrument manufactured by Hitachi, Japan, operating at voltage levels of 15 kV and magnifications of 400X and

1000X [75], [76]. This analysis allowed detailed observation of the samples' structure and morphological characteristics, helping to understand how torrefaction and other processes affect the physical properties of biomass.

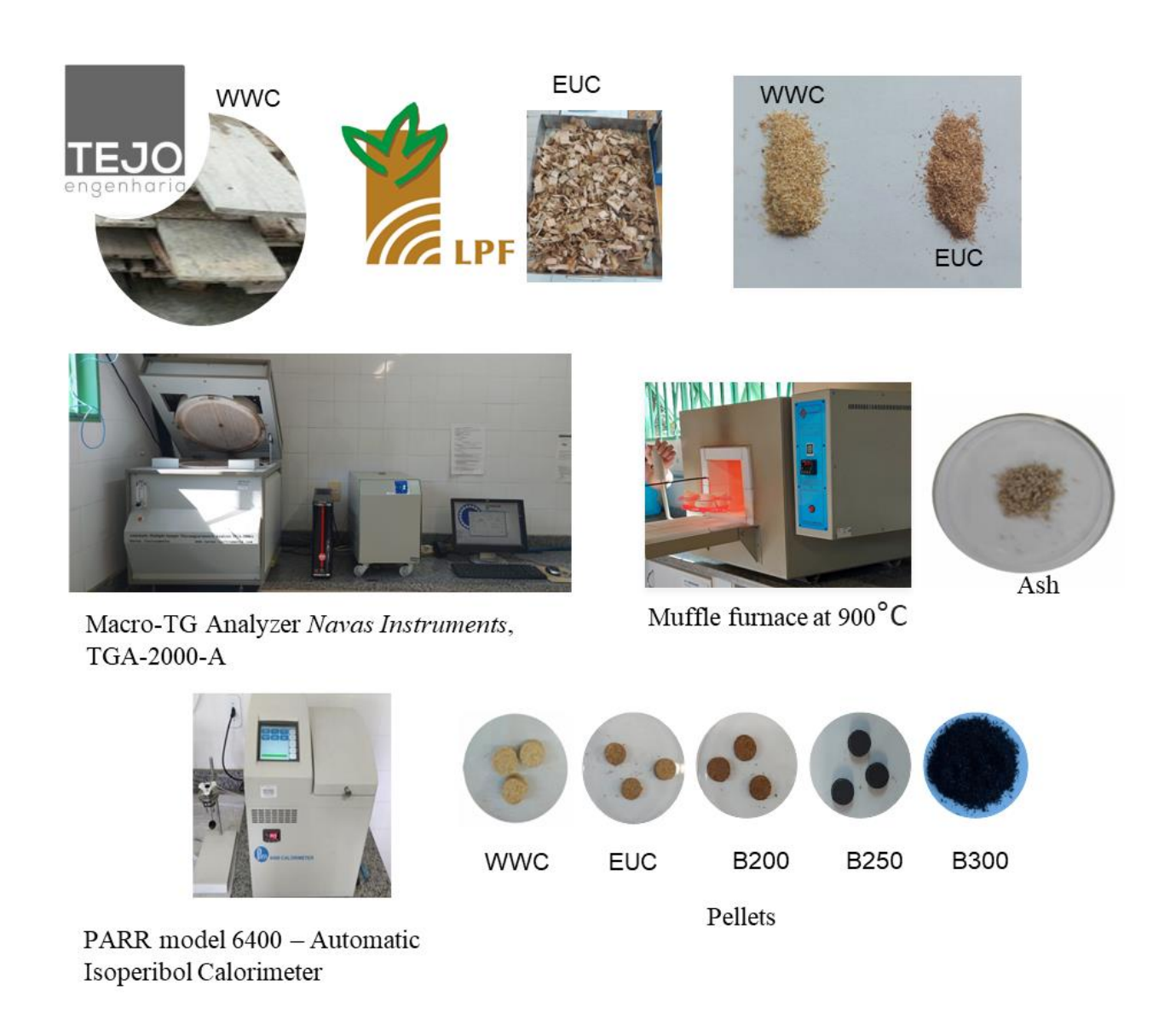


Figure 5. Samples and Analyses (Blend CWW and EUC). (Font: Author).

# 3.3 TORREFACTION

# 3.3.1 Torrefaction experiments

The torrefaction treatment was operated in triplicates. The tests were performed for samples of 1.2±0.05 g in alumina crucibles with a thermogravimetric analyzer (Macro-TG Analyzer *Navas* 

*Instruments*, TGA-2000-A), detailed in previous literature [77]. The TG experimental error was controlled below 0.5%. A linear heating rate of 20 °C min<sup>-1</sup> was imposed from room temperature to 105 °C and maintained isothermally for 30 min to ensure dry conditions. The treatment severity was established for light (200 °C), mild (250 °C) and severe (300 °C) in an inert atmosphere with a constant flow rate (3 L min<sup>-1</sup>) of nitrogen gas (99.2%) and a heating rate of 7 °C min<sup>-1</sup>. After the drying, the samples were heated until the treatment temperature and isothermally held for 50 min of treatment.

### **3.3.2** Torrefaction performance

Four torrefaction performance indexes were assessed according to Table 5. Chen et al. [78] proposed the TSI, an index to evaluate the extent of biomass degradation during torrefaction. The TSI, explored in previous works [79], [80], [81], [82], is a dimensionless parameter floating from 0-1 calculated with Eq. (6) (Table 5). The TSI is the ratio between the normalized  $SY(t)_T$  reduction (due to increasing temperature and time) and the solid yield of the severest treatment condition (in the present work  $SY(50)_{300}$ , T=300 °C, and t=50 min) [82].

Table 5. Formulation of the four torrefaction severity indexes.

Index	Formulation	Eq.	Ref.
Yield property-based			
Solid yield (wt.%)	$SY(t)_{T_H} = \frac{w_i(t)}{w_0} \times 100$	(6)	[83]
Torrefaction severity index	$TSI = \frac{100 - SY(t)_{T_H}}{100 - SY(50)_{300}}$	(7)	[82]
Index of torrefaction	$I_{torr} = \frac{HHV_{torrefled}}{HHV_{raw}}$	(8)	[84], [85]
Operating condition-based			
Dimensionless torrefaction	$log\left[t^{\alpha} \times exp\left(\frac{T_H}{14.75}\right)\right]$		
severity factor	$TSF_{dim} = rac{log\left[t^{lpha} imes exp\left(rac{T_{H}}{14.75} ight) ight]}{log\left[50^{lpha} imes exp\left(rac{300}{14.75} ight) ight]}$	(9)	[13]

 $w_i(t)$  is the instantaneous weigh loss in grams,  $w_0$  is the initial weight in grams, t is the treatment time (in min),  $T_H$  is the reaction temperature (in °C), and HHV is the higher heating value in MJ kg<sup>-1</sup>.

The index of torrefaction  $(I_{torr})$  [84], [85] or enhancement factor [82] is an index built on the ratio of the torrefied output product's HHV to raw biomass HHV determined with Eq. (8) (Table 5). Another torrefaction index is the dimensionless torrefaction severity factor, a modification of the

torrefaction severity factor. Chen et al. [86] first proposed the TSF and detailed derivation was presented in the previous studies [82], [86]. This severity index was proposed to account for the relationship between operating conditions of torrefaction where, in the present investigation, t is the treatment time (50 min) and  $T_H$  is the reaction temperature (200, 250, and 300 °C).

The TSF also considers the biomass nature and its intrinsic sensitivity to thermal degradation by introducing the exponential factor  $\alpha$ , which must be calculated [86]. An optimum value for  $\alpha$  can be obtained via the linear correlation between WL and TSF [86]. The coefficient of determination  $R^2$  varies when altering the time exponent  $\alpha$ , and the alpha optimum is obtained for the higher value of  $R^2$ . Its dimensionless form was first presented in [13] and can be calculated with Eq. (9) (Table 5). The  $TSF_{dim}$  is appealing because it allows proper comparison with SY and TSI indexes, which vary in the same range of 0–1. The indicators energy yield  $(EY^{(T)})$  and the energy mass-coefficient -index (EMCI), defined by Eqs. (10) and (11) were also explored.

$$EY^{(T)} = S_Y^{(T)} \times I_{torr} \tag{10}$$

$$EMCI = EY^{(T)} - S_{\nu}^{(T)} \tag{11}$$

In addition, the Specific Chemical Bioexergy (SCB) is a vital indicator of biofuel characterizations for the torrefaction process [87]. The SCB offers the actual energy contained within the torrefied biofuel, which can be calculated based on the data of some chemical compounds in biofuel [87]. A prior investigation explored 86 biomass varieties, revealing that dry biomass's chemical exergy spans from 11.5 to 24.2 MJ kg<sup>-1</sup>, consistently slightly higher than the HHV (db) [88]. Their approach was based on Szargut's reference environmental model [87], which is tailored specifically to biomass and accounts for all elements commonly analyzed in the ultimate analysis. Given its relatively minor impact, considerations such as inorganic matter, ash chemical exergies and entropy changes in ash formation can be discounted. The average ratio reported for specific chemical exergy to HHV for dry biomass was 1.047. Hence, Eq. (12), an empirical equation proposed by [83] based on HHV, has been utilized here to determine the SCB.

$$SCB = 1.047 \times HHV \tag{12}$$

The  $I_{torr}$  and SCB are tied to biomass HHV.  $I_{torr}$  sheds light on treatment effects on HHV quality, while SCB factors in exergy, enabling accurate comparisons for exergy efficiency analysis. Furthermore, the EMCI compares EY and SY, striving for higher EY and lower SY, correlating biofuel quality to thermal degradation severity and HHV improvement.

### 3.3.3 Torrefaction kinetics

The presence of higher ash content in CWW may exert an influence on the kinetics of torrefaction reactions. Therefore, kinetic modeling was applied here to predict thermal degradation behavior. The numerical routine was built on the two-step consecutive reaction model [89]. This model was selected since it reported a high precision and simplicity for a broad range of torrefaction operational parameters (particle size, temperature, heating rate, and holding time) [57], [58], [59], [60], [61], [62], [64], [90], [91], [92], [93], [94], reactor atmosphere (inert and oxygen-lean conditions [95], [96]), type of biomass samples (individual species [97], [98], a blend of lignocellulosic biomasses [13] or even separated wood components [99]), and also catalytic conditions [100], [101].

The consecutive two-step reactions model (Eq. (13)) was structured based on the three-stage approach [102], [103] and validated in the previous numerical simulations works [98], [100]. Model details are presented in previous works [98], [100].

$$1^{\text{st}} \text{ reaction step: } \begin{cases} A \overset{k_1}{\to} B \\ A \overset{k_{V_1}}{\to} V_1 \end{cases}$$

$$2^{\text{nd}} \text{ reaction step: } \begin{cases} B \overset{k_2}{\to} C \\ B \overset{k_{V_2}}{\to} V_2 \end{cases}$$

$$(13)$$

The model consists of first-order mechanics evolving through two reaction steps. The first step (Eq. (13)) is attributed to the hemicelluloses conversion into light volatiles and the removal of extractives [104], being described by the decomposition of A in B, releasing  $V_1$ . Meanwhile, the second step is attributed to the conversion of B into C, releasing  $V_2$ , characterizing the degradation of remanescent hemicelluloses, cellulose, and part of lignin [104]. Consequently, the two-step model is suitable for simulating biomass degradation during torrefaction treatment. The pseudo component A is ascribed to the raw biomass feedstock (100% of the sample SY) at the beginning of the treatment (t = 0). The kinetic rate  $k_i$  (min<sup>1</sup>,  $i = 1, 2, V_1, V_2$ ), defined by the Arrhenius law, was determined using Eq. (14) [102].

$$k_i = A_0 i \exp\left(\frac{-E_a i}{RT}\right) \tag{14}$$

where  $A_0i$  (min<sup>-1</sup>) is the pre-exponential factor,  $E_ai$  (J mol<sup>-1</sup>) is the activation energy, R is the universal gas constant, and T (K) is the temperature [89].

The solid  $(k_1, k_2)$  and volatile  $(k_{V_1}, k_{V_2})$  reaction rates for the CWW and *Eucalyptus* blend were determined by fitting SY experimental curves to predicted ones [78]. The model considers the heating and isothermal stages for calculation. The solver (function "fminsearch" of Matlab® software) is based on the Nelder-Mead optimization algorithm, which is employed to minimize the mean root square of the difference  $(diff^T(t))$  between experimental  $(S_{Y,exp}^{(T)}(t))$  and calculated  $(S_{Y,calc}^{(T)}(t))$  solid yields, as expressed in Eq. (15). The calculation is considered convergent and thus stopped when the absolute difference of  $diff^T(t)$  value between two iterations is smaller than  $10^{-4}$  [103].

$$diff^{T}(t) = \sqrt{\sum_{t} \left( \frac{S_{Y,exp}^{(T)}(t) - S_{Y,calc}^{(T)}(t)}{S_{Y,exp}^{(T)}(t)} \right)^{2}}$$
 (15)

### 3.4 COMBUSTION BEHAVIOR

The combustion experiments were performed for raw (CWW, *Eucalyptus*, and blend) and torrefied (B200, B250 and B300) material. Combustion experiments were conducted in duplicate (relative error was controlled below 3%) with an SDT Q600 TGA, TA Instruments. The samples (5 ± 0.1 mg), with a particle size of 100 mesh (0.145 mm), were heated from room temperature (25 °C) at a heating rate of 20 °C·min<sup>-1</sup> to 105 °C. The temperature was maintained at 105 °C for 5 min to provide a dry basis. The samples were then heated to 800 °C at a heating rate of 20 °C min<sup>-1</sup> and 100 mL min<sup>-1</sup> flow of synthetic air (80% N₂ and 20% O₂) [105].

Within this investigation, the ignition temperature ( $T_i$  in °C) was defined as the temperature at which the combustion rate escalated to 1% min<sup>-1</sup> during the onset of a significant combustion event. The burnout temperature ( $T_f$  in °C), on the other hand, was designated as the temperature at which the combustion rate reduced to 1% min<sup>-1</sup> upon conclusion of a combustion process [106], [107], [108], [109]. The peak temperature  $T_p$  (°C) is defined as the temperature of the maximum DTG value ( $DTG_{max}$ ). The combustion behavior was evaluated based on the ignition index  $D_i$  (% min<sup>-3</sup>) and burnout index  $D_f$  (% min<sup>-4</sup>) Eqs. (16) and (17).

$$D_i = \frac{DTG_{max}}{t_p \times t_i} \tag{16}$$

$$D_f = \frac{DTG_{max}}{\Delta t_{1/2} \times t_p \times t_f} \tag{17}$$

Here  $t_i$ ,  $t_p$  and  $t_f$  (min) are attributed to the time in which the ignition, peak, and burnout temperatures occur, respectively.  $\Delta t_{1/2}$  is the time range of  $DTG/DTG_{max} = 0.5$ .

### 3.4.1 Potential CO<sub>2</sub> retention

The estimation of the CO<sub>2</sub> amount that would be retained using renewable fuels (potential CO<sub>2</sub> retention) instead of fossil fuels was made to verify the environmental advantages of using residue CWW and *Eucalyptus* blend as renewable fuels within urban districts. The CO<sub>2</sub> mass (kg CO<sub>2</sub>) potentially avoided from fossil fuels can be determined as a function of the emission factor (EF, in kg.CO<sub>2</sub> L<sup>-1</sup>) and the Equivalent volume (EV, in L m<sup>-3</sup>) of fossil fuel per cubic meter of biomass (Eq. (18)).

$$Potential CO_2 retention = EF \times EV$$
 (18)

Here, the EF is ascribed to the reference liquid fossil fuels, which include petroleum (3.43 kg.CO<sub>2</sub>.L<sup>-1</sup>), diesel fuel (3.53 kg.CO<sub>2</sub>.L<sup>-1</sup>), fuel oil (2.94 kg.CO<sub>2</sub>.L<sup>-1</sup>), and gasoline (3.94 kgCO<sub>2</sub>.L<sup>-1</sup>) [84]. Meanwhile, the Equivalent volume (EV) of fossil fuel (liters per cubic meter, L.m<sup>-3</sup>) per cubic meter of biomass (Eq. (19)) is ascribed as the amount of fossil fuel that is required to produce the same amount of energy produced by biomass [110], [111].

Here, the *Bioenergy density*<sub>biomass</sub> (MJ m<sup>-3</sup>) (Eq. (20)) measures how much energy a substance releases during complete combustion per unit of volume [110], [111], [112]. Therefore, for the investigated biomass herein it is determined as a function of bulk density (kg m<sup>-3</sup>) and  $LHV_{bio}$  (MJ kg<sup>-1</sup>) (Table 5). Meanwhile, the *Energy density*<sub>fossifuels</sub> of the liquid fossil fuels were 37.03, 36.27, 39.93, and 32.62 GJ m<sup>-3</sup> for petroleum, diesel fuel, fuel oil, and gasoline, respectively [110], [111].

$$EV = \frac{Bioenergy\ density_{biomass}}{Energy\ density_{fossifuels}} \times 1000 \tag{19}$$

Bioenergy density<sub>biomass</sub> = Bulk density 
$$\times$$
 LHV<sub>bio</sub> (20)

# 4 RESULTS AND DISCUSSIONS

This section presents the main results obtained from the torrefaction of construction wood waste (CWW) mixed with *Eucalyptus sp*. The torrefaction treatments were carried out at three different temperatures (200°C, 250°C, and 300°C) to evaluate the impact of process severity on the physical, chemical, and energetic properties of the biomass. Parameters such as solid yield, ash content, heating value, torrefaction kinetics, combustion behavior, and energy equivalence in relation to fossil fuels were analyzed. These results provide valuable insights into the technical and environmental feasibility of using CWW as a raw material to produce high-quality solid biofuels.

#### 4.1 CHEMICAL PROPERTIES AND ENERGETIC PARAMETERS

# 4.1.1 Feedstock quality

Proximate analysis is essential to provide information on ash content, volatile matter, and fixed carbon and insights into the combustion behavior of fuels. Table 6 shows the proximate values for the feedstock (CWW and *Eucalyptus*).

Table 6. Energetic		-1	- £ 41	
Table b. Energence	ana nnysicai	cnaracterization	Of the raw	materials blend

Specie	CWW	EUC	Standards
MC (%)	10.61±0.11	$8.97 \pm 0.06$	
Proximate (%)			
Ash	$1.48 \pm 0.05$	$0.67 \pm 0.03$	ISO 18122-2015
VM	$82.48\pm0.18$	$85.27 \pm 0.79$	ISO 18123-2015
FC <sup>a</sup>	$16.04\pm0.18$	14.06±0.79	
Fuel ratio <sup>b</sup>	$0.2\pm0.07$	$0.16\pm0.08$	
Ultimate (%)			ASTM E777/2008 and E778/2008
C	$44.65\pm0.15$	$44.70\pm0.48$	Perkin Elmer analyzer
Н	$6.07\pm0.01$	$5.82\pm0.20$	
N	$0.14\pm0.06$	$0.09\pm0.02$	
$O_p$	47.67±0.10	$48.73 \pm 0.27$	
H/C ratio	$1.63\pm0.01$	$1.56 \pm 0.06$	
O/C ratio	$0.80\pm0.00$	$0.82\pm0.01$	
Calorific			
HHV	$20.10\pm0.03$	$19.42 \pm 0.03$	ISO 18125:2017
LHV	$18.73 \pm 0.05$	$18.12 \pm 0.05$	PARR model 6400 calorimeter
SCB d	21.04±0.03	20.33±0.03	

<sup>&</sup>lt;sup>a</sup> by difference (FC = 100 − VM − ash); <sup>b</sup> FR=FC VM<sup>-1</sup>, <sup>c</sup>O = 100 − C − H − N − ash; <sup>d</sup> Specific Chemical Bioexergy.

Regarding feedstock, CWW (contaminated *Pine*) and *Eucalyptus sp*. wood revealed 16.12 and 14.06% for FC, 82.40 and 85.27% for VM, and 1.48 and 0.67% for ash content, respectively. Considering *Eucalyptus* feedstock, results align with the literature [113], [114], [115] that evaluated *Eucalyptus* sp., *Eucalyptus grandis* and blended *Eucalyptus urophylla and Eucalyptus grandis* species and reported proximate values raging between 15.30–15.90%, 81–84%, and 0.1–0.70% for FC, VM, and ash content, respectively. Uncontaminated *Pine* was characterized in literature [116], [117], [118], reporting FC, VM, and ash content between 15.17–16.08%, 77.71–84.19%, and 0.3–0.63%, respectively. The literature on separated feedstock corroborates Table 6, except for the ash content, exhibiting higher values, as expected, since CWW presents traces of cement, mortar, soil, and gypsum, among others. Moreover, past studies assessed activities construction and demolition wood waste [14], [119], [120], showing FC, VM and ash ranging between 12.3–21.0%, 77.7–85.7%, and 1.33–2%, respectively, in line with Table 6.

Regarding the ultimate results of *Eucalyptus* and CWW feedstocks, H/C and O/C ratios were 1.56–1.63 and 0.82–0.80, respectively. The results are consistent with the literature, in which H/C and O/C ratios ranged between 1.49–1.67 and 0.68–0.80 for untreated *Eucalyptus* [3], [113], [118] and ranged between 1.64–1.69 and 0.67–0.73 for untreated *Pine* [3], [113], [118]. HHV is intrinsically related to the ultimate and proximate contents. CWW and *Eucalyptus* sp. presented an HHV of 20.10 and 19.42 MJ kg<sup>-1</sup>. Results align with *Pine* and *Eucalyptus* shavings from previous literature that presented HHV of 20.37 and 19.14 MJ kg<sup>-1</sup> [110]. Moreover, wood waste from the industrial, construction, and demolition industries presented HHV between 19.2–21.10 MJ kg<sup>-1</sup> [2], [14], [114], agreeing with the 20.10 MJ kg<sup>-1</sup> of CWW (Table 6).

### 4.1.2 Raw and torrefied blends

Table 7 shows the properties of raw and torrefied blends. In addition, the Ternary diagram of proximate results and the Van Krevelen diagram are displayed in Fig. 6, highlighting their differences and changes according to torrefaction severity (light, mild, and severe) and allowing comparison with the literature. The aim of blending CWW with *Eucalyptus* (a wood species with lower ash content) was to reduce the ash content of the obtained blend. Comparing CWW (see Table 6) with B (raw) (Table 7), a decrease in ash content (from 1.48% to 1.08%) and fixed carbon (from 16.12 to 15.04%) was observed, while volatile matter increased (from 82.40 to 83.88%), as expected. Additionally, a slight variation in H/C and O/C ratios was noticed.

Table 7.Properties of the raw (B) and torrefied blends (B200, B250 and B300). Proximate (volatile matter (VM), fixed carbon (FC), and ash content in %), ultimate (CHON in %), and calorific (LHV, HHV and SCB in MJ kg-1) analysis. Torrefaction performance index (SY, TSI, TSF, I\_torr, EY, EMCI and Bioenergy density).

Specie	B (raw)	B200	B250	B300				
Proximate analysis (%) <sup>a</sup>								
Ash	$1.08\pm0.03$	$1.05 \pm 0.02$	$1.24\pm0.02$	$1.77 \pm 0.01$				
VM	$83.88 \pm 0.01$	$83.64 \pm 0.05$	$76.48 \pm 0.13$	53.81±0.67				
FC	$15.04 \pm 0.07$	$15.31 \pm 0.05$	$22.28\pm0.13$	$44.42 \pm 0.67$				
Fuel ratio <sup>b</sup>	$0.18\pm0.03$	$0.18 \pm 0.02$	$0.29\pm0.02$	$0.83 \pm 0.02$				
Ultimate (%) <sup>a</sup>								
C	$44.68 \pm 0.25$	$45.62 \pm 0.01$	$47.39\pm0.16$	59.71±0.05				
Н	$5.95\pm0.10$	$5.62 \pm 0.11$	$5.41\pm0.12$	$4.09\pm0.05$				
N	$0.12\pm0.03$	$0.09\pm0.02$	$0.26 \pm 0.04$	$0.25 \pm 0.01$				
O c	48.20±0.14	$48.68 \pm 0.09$	46.95±0.32	35.96±0.16				
H/C ratio	$1.60\pm0.03$	$1.49 \pm 0.03$	$1.38\pm0.03$	$0.83 \pm 0.01$				
O/C ratio	$0.81 \pm 0.01$	$0.81 \pm 0.00$	$0.75\pm0.01$	$0.46 \pm 0.00$				
Physical (kg m <sup>-3</sup> )								
Bulk density	302.98±0.06	316.57±0.48	326.58±0.30	$246.57 \pm 0.51$				
Calorific (MJ kg <sup>-1</sup> )								
HHV	$19.76 \pm 0.03$	19.98±0.01	20.76±0.01	$24.10\pm0.00$				
LHV	$18.42 \pm 0.03$	$18.71 \pm 0.03$	19.53±0.03	$23.18\pm0.01$				
SCB d	$20.69 \pm 0.03$	$20.92 \pm 0.02$	$21.74 \pm 0.01$	$25.23 \pm 0.00$				
<b>Performance Indexes</b>								
SY (%)	$100\pm0.00$	$98.42 \pm 0.05$	$86.88 \pm 0.15$	$62.66 \pm 0.70$				
TSI	0	0.04	0.37	1.00				
TSF	-	0.81	0.90	1.00				
$I_{torr}$	-	$1.011 \pm 0.00$	$1.05\pm0.00$	$1.22 \pm 0.00$				
EY (%)	$100\pm0.00$	$99.52 \pm 0.08$	91.25±0.19	$76.43 \pm 0.85$				
EMCI	-	$1.10\pm0.10$	4.37±0.24	13.77±1.10				
Bioenergy density e	5.58±0.03	5.92±0.10	6.38±0.09	5.72±0.12				

<sup>&</sup>lt;sup>a</sup> % based on dry mass – db; <sup>b</sup> FC VM<sup>-1</sup>, <sup>c</sup> O=100–C–H–N–ash, <sup>d</sup> calculated by Eq. (12); <sup>e</sup> in GJ m<sup>-3</sup> calculated by Eq. (20). Source: Barbosa et al., (2024) [71]

During torrefaction, distinct reaction mechanisms such as decarboxylation, dehydration, and demethylation occur for each lignocellulosic component [121]. As torrefaction severity increases, the dehydration process of biomass releases moisture and light volatiles more rapidly and extensively, resulting in a decrease in volatile matter (VM) and, consequently, an increase in the concentration of ash and FC [59], [122], [123].

Figure 6(a) shows the ternary diagram of proximate results. The results demonstrate that with an increased torrefaction severity, there was a significant increase in FC ranging from 15.04–44.42%,

representing an increase of 1.8, 47.81, and 192.28%, and a decrease in VM ranging from 83.88–53.81%, indicating a reduction of 0.3%, 8.82%, and 35.85% for samples B200, B250, and B300, respectively, compared to B.

The experimental characterization of the torrefied product revealed an ash content ranging from 1.05% to 1.77%, which increased with torrefaction temperature. The diagram shows that as torrefaction severity increases, data move to the up corner (mainly due to the higher FC and lower VM, increasing FR up to 0.83). Results are in line with raw and torrefied products of *Pinus radiata* (P) (raw, 250 and 280 °C [118]), Demolition wood residues (DW) (raw, 250, 270, and 300 °C [14]), Blend composed of construction and demolition wood (DC) and municipal solid waste (MSW) (raw and 220 °C [2]), Blend composed of construction and demolition wood (DC) and refuse-derived fuel (RDF) (raw and 220 °C [2]), *Pinus elliottii* (P) (raw, P300 and 300 °C [124]), *Eucalyptus* sp. (E). (raw, 240, 260, and 280 °C [113]).

Figure 6(b) exhibits the Van Krevelen diagram. The H/C and O/C atomic ratios help evaluate raw and torrefied biomass's upgrade and aromatization levels. Moreover, it provides a graphical evaluation comparing raw biomass and obtained torrefied products with literature data and fossil fuels (Coal, Lignite, and Peat) characteristics regions. Throughout the torrefaction process, different reactions occur for each lignocellulosic material component. These reactions include decarboxylation, dehydration, and demethylation [91]. The reductions in the H/C and O/C ratios confer greater structural stability and a higher degree of carbonization [125].

Hemicelluloses conversion occurs within 220–280 °C [122], [123]. This process involves removing water (dehydration) and breaking weak bonds between small attached groups and the leading polymer chains [91]. In addition, when cellulose undergoes dehydration at approximately 200 °C, the primary product released is water. As temperatures increase to around 280 °C, additional products such as CO, CO<sub>2</sub>, and small organic compounds are also released [126]. During torrefaction, lignin gradually and partially degrades, which starts at about 200 °C. Dehydration reactions involving the hydroxyl groups on the phenolic rings of lignin occur at lower temperatures [92].

Figure 6(b) visually demonstrates the prevalence of dehydration (more noticeable in B300) and decarboxylation (leading to the formation of H<sub>2</sub>O, CO<sub>2</sub>, and CO) as the primary reaction mechanisms. The ratios of hydrogen to carbon (H:C) and oxygen to carbon (O:C) ranged between 1.60–0.83 and 0.81–0.46 (Table 7), encompassing both the original biomass and the resulting torrefied products. These findings align with earlier torrefactions experiments conducted on *Eucalyptus sp.* (E). (raw, 240, 260 and 280 °C [113]) and *Pinus radiata* (P) (raw, 250, and 280 °C

[118]), which resulted in H/C ratios of 1.0 and 1.42, and O/C ratios of 0.37 and 0.55, respectively. It can be observed that the severe torrefaction treatments (B300) positions move toward the corner of the diagram, a region characteristic of fossil fuels, demonstrating the coalification processes and enhanced properties that torrefaction confers to raw biomass as biofuel.

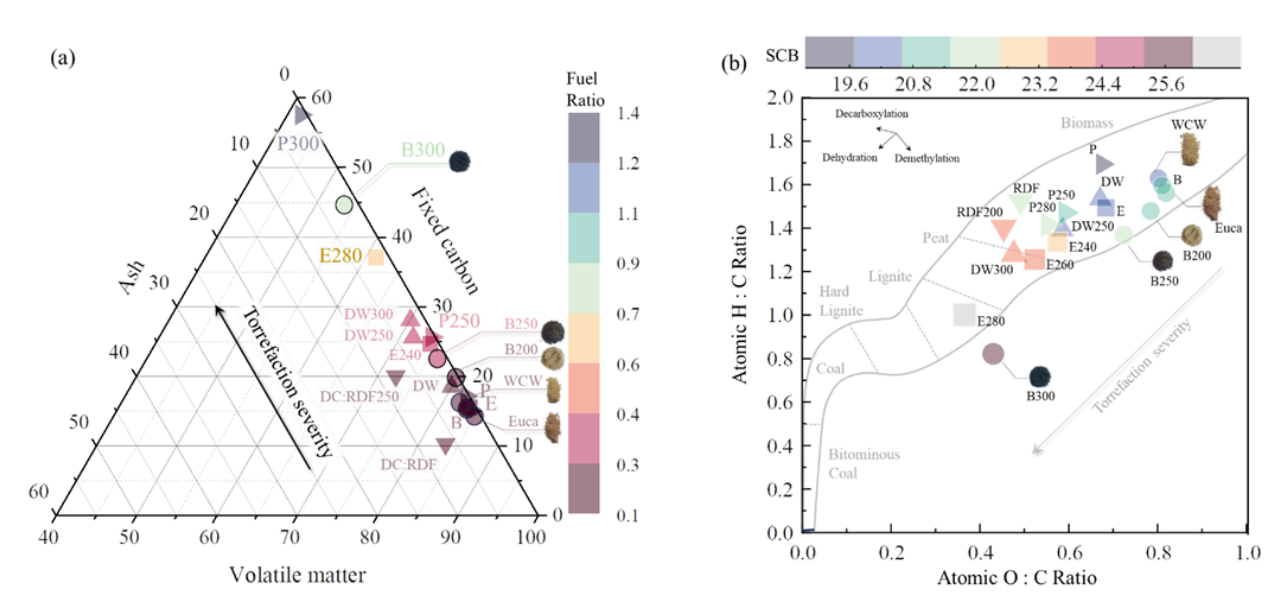


Figure 6. Ternary diagram of proximate analysis for *Eucalyptus*, CWW, B, B200, B250 and B300. (b) Van Krevelen diagram. Data for comparison: *Pinus Radiata* (P–raw, 250, 280 °C [118]), Demolition wood residues (DW–raw, 250, 270 and 300 °C [14]), Blend composed of c construction and demolition wood (DC) and refuse-derived fuel (RDF–raw and 220 °C [2]), *Pinus elliottii* (P–raw and 300 °C [124]), *Eucalyptus* sp. (E–raw, 240, 260 and 280 °C [113]. Source: Barbosa et al., (2024) *[71]* 

The presence of polar groups like carboxyl, carbonyl, and hydroxyl in the structure of raw biomass contributes to its lower higher heating value (HHV) [93]. After torrefaction treatment, HHV values varied between 19.98–24.10 MJ kg<sup>-1</sup>, increasing with torrefaction severity. The results are consistent with 250 and 300 °C torrefaction conducted on construction and demolition wood waste, where the HHV varied from 20.3 to 22.5 MJ kg<sup>-1</sup> [14]. Furthermore, results align with torrefied *Eucalyptus* (240 to 280 °C), in which HHV ranged from 21.8 to 25 MJ kg<sup>-1</sup> [113], 300 °C torrefied agricultural residues, including betel nutshells, palm fiber, and coconut fiber (HHV ranged between 23.48–25.29 MJ kg<sup>-1</sup>) [127], and with torrefied *Pinus elliotti* at temperatures of 200 to 300 °C (HHV varied between 20.7–28.9 MJ kg<sup>-1</sup> [124]). The SCB indicates the net energy in the biofuel derived from biomass [87], which varied between 20.69–25.23 MJ kg<sup>-1</sup>. Compared to raw biomass, the total SCB of the biofuel (B300) increased to 21.94%, from 20.69 MJ kg<sup>-1</sup> (raw) to 25.23 MJ kg<sup>-1</sup> after the torrefaction.

For treatments B200, B250, and B300 (Table 7), EY varied between 99.55–76.76%, decreasing with torrefaction severity due to the SY reduction. The EY results indicate an excellent blend quality as they retain about 70% to 90% of the initial energy content [59]. A better indicator to evaluate torrefaction influence on the energetic upgrade of raw biomass is the EMCI, which varied between 1.10–13.77.

The bioenergy index, also called energy density, evaluates the potential bioenergy obtained from a specific biomass volume [34]. This indicator establishes a connection between the density of the material and its HHV (displayed in Table 7), essentially quantifying the energy per volume unit. The bioenergy densities achieved for the original mix (B) and torrefied mixtures (B200, B250, and B300) are presented in Table 7.

The torrefaction treatment reduces the biomass particle size, leading to higher bulk density. This outcome arises from decreased empty spaces between particles [127]. Compared to raw material (302.98 kg m<sup>-3</sup>), the bulk density increased by 4.49 and 7.79% for B200 (316.57 kg m<sup>-3</sup>) and B250 (326.58 kg m<sup>-3</sup>) torrefaction, as expected. Nevertheless, a reduction was observed for the B300 (246.57 kg m<sup>-3</sup>). This behavior might be attributed to the particle size reduction during thermal treatment, in which the mass loss is smaller than the volumetric contraction. This behavior was also reported in the study conducted by Phanphanich, M., & Mani, S. [128], which evaluated the torrefaction treatment of *Pine* chips and logging residues.

Table 7 displays the Bioenergy density (GJ m<sup>-3</sup>) of raw (B) and torrefied (B200, B250, and B300). The raw blend exhibited a bioenergy index of 5.58 GJ m<sup>-3</sup>, superior to other lignocellulosic biomass materials such as Ponkan peel (4.42 GJ m<sup>-3</sup>), cotton stalk (5.08 GJ m<sup>-3</sup>), and rice husk (3.40 GJ m<sup>-3</sup>) [129], [130], [131]. Considering torrefied samples, the bioenergy index increased by 6 and 14% for B200 and B250, following the bulk density and LHV increase (see Table 7). Since the bulk density of B300 was reduced, the bioenergy index for B300 was lower than B200 and B250, following the order: B250>B200>B300>B.

These findings underscore the significance of incorporating supplementary performance indices in assessing the impact of torrefaction treatment on fuel quality. The heightened bioenergy density shown here highlights the potential to generate substantial heat per biomass unit volume. This metric not only mitigates transportation expenses but also amplifies storage capabilities.

Torrefied fuels exhibit a higher percentage of carbon and increased energy density, which will enhance the efficiency of combustion equipment utilization (as well as prolong the combustion duration owing to the higher FC concentration) [132]. The higher energy density reduces firewood

consumption and facilitates the operation of boilers. For example, if a boiler with an energy consumption rate of 10.4 GJ  $h^{-1}$  [133] is supplied with the torrefied product, 431.54 kg  $h^{-1}$  of B300 is required instead of 526.32 kg  $h^{-1}$  of B(raw).

Figures 7 and 8 display the correlations and the  $R^2$  values between torrefaction performance indexes (SY, TSI,  $I_{torr}$ , and TSF) and proximate (fuel ratio – FC/VM and ash), ultimate (H/C and O/C) and energetic (HHV and EMCI) properties. A linear behavior between the severity indexes and torrefied product properties was evidenced, aligning with previous studies on wood torrefaction [82]. All evaluated indexes evidenced a high coefficient of correlation ( $R^2$ > 0.8908), and  $I_{torr}$  reported a superior  $R^2$ >0.99 for all evaluated properties.

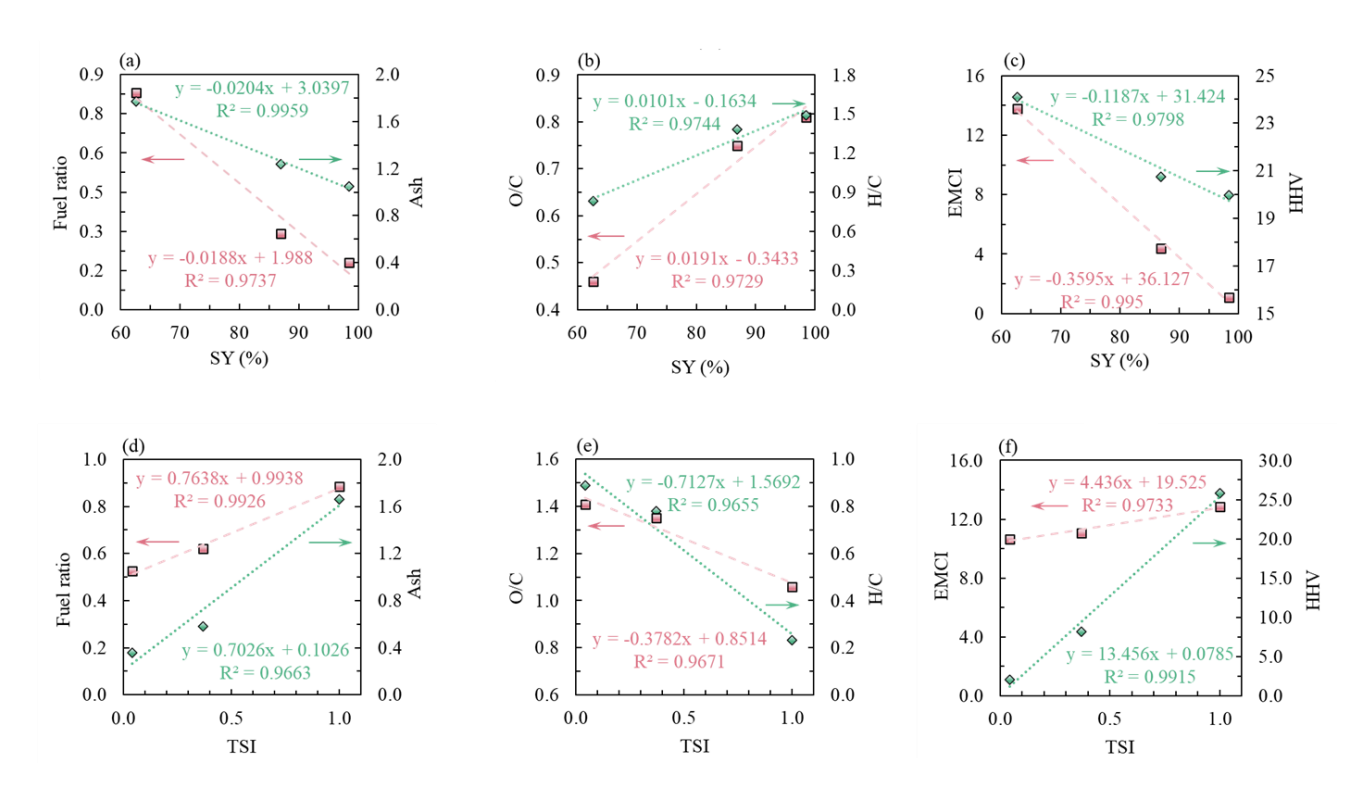


Figure 7.Linear correlation between SY and TSI and proximate analysis ((a) and (d)), ultimate analysis ((b) and (e)), and calorific analysis ((c) and (f) Source: Barbosa et al., (2024) [71].

### 4.2 PHYSICAL CHANGE

The color change of biomass during torrefaction results from a series of complex chemical processes, including thermal degradation, oxidative reactions, and transformations in the composition of lignocellulosic components [10], [50], [63]. Regarding Fig. 9, the color change of B200 was less

pronounced. Conversely, B250 and B300 showed evident color modification, suggesting the effectiveness of the torrefaction.

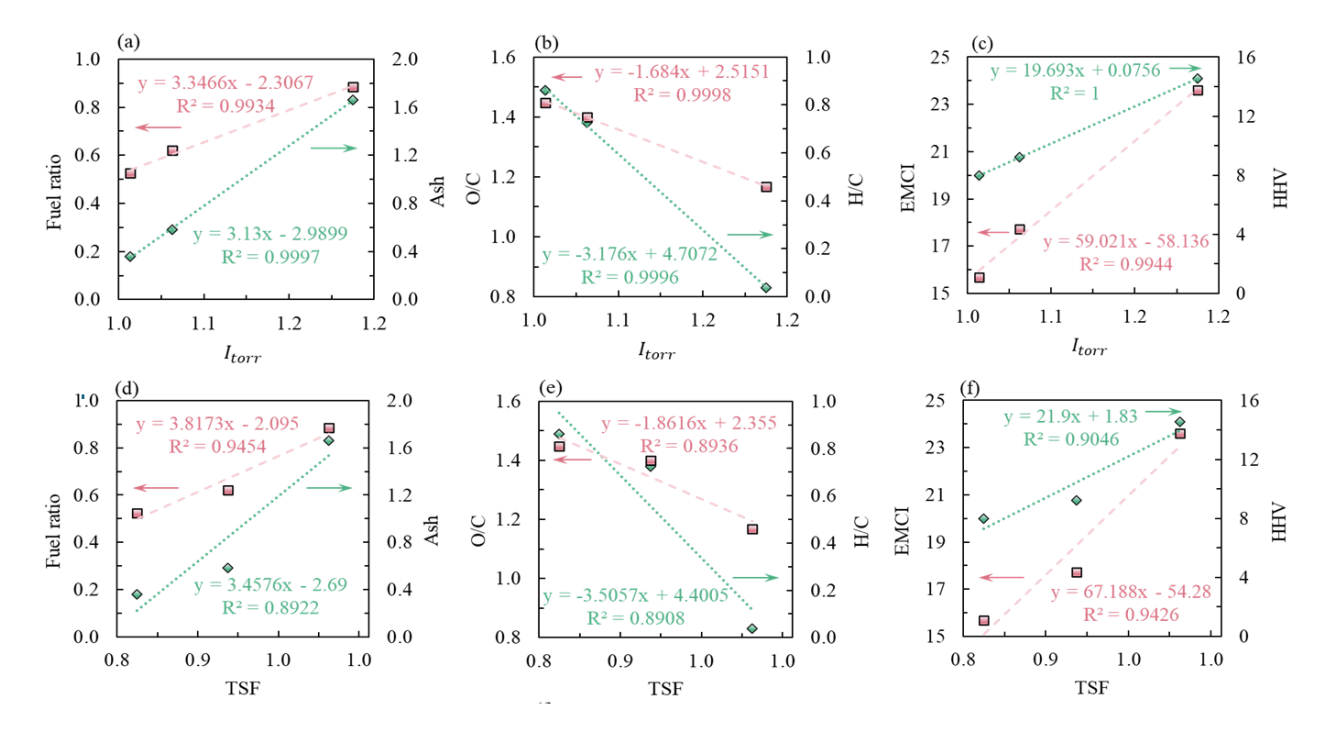


Figure 8. Linear correlation between indexes ( $I_{torr}$  and TSF) and proximate analysis ((a) and (d)), ultimate analysis ((b) and (e)), and calorific analysis ((c) and (f). Source: Barbosa et al., (2024) [71]

Through the analysis of the biomass morphology images in Fig. 9, the red circles indicate the presence of cement contamination in both the torrefied (B200, B250, and B300) and CWW samples. Figure 9 also visually depicts the physical surface characteristics of raw (*Eucalyptus* and CWW) and torrefied materials.

The raw materials display a smooth exterior in contrast to the notably altered surface of the torrefied samples. However, subjecting the samples to torrefaction at 200 °C does not significantly transform the surface morphology compared to the untreated samples, as evidenced by the color change. This behavior implies that releasing volatile substances at this temperature minimally influences the inherent surface structure. In contrast, torrefaction conducted at 250 °C and 300 °C promoted changes in the surface structure, evidenced by heightened gaps and fissures in both B250 (Fig. 9(d)) and B300 (Fig. 9(e)).

B300 exhibits more fissures than B250, indicating that elevated temperatures intensify the modification of surface characteristics. These modifications in surface features can be attributed to

the dissipation of volatile components, the entrapment of gases during the elimination of volatiles, and the degradation of holocellulose.

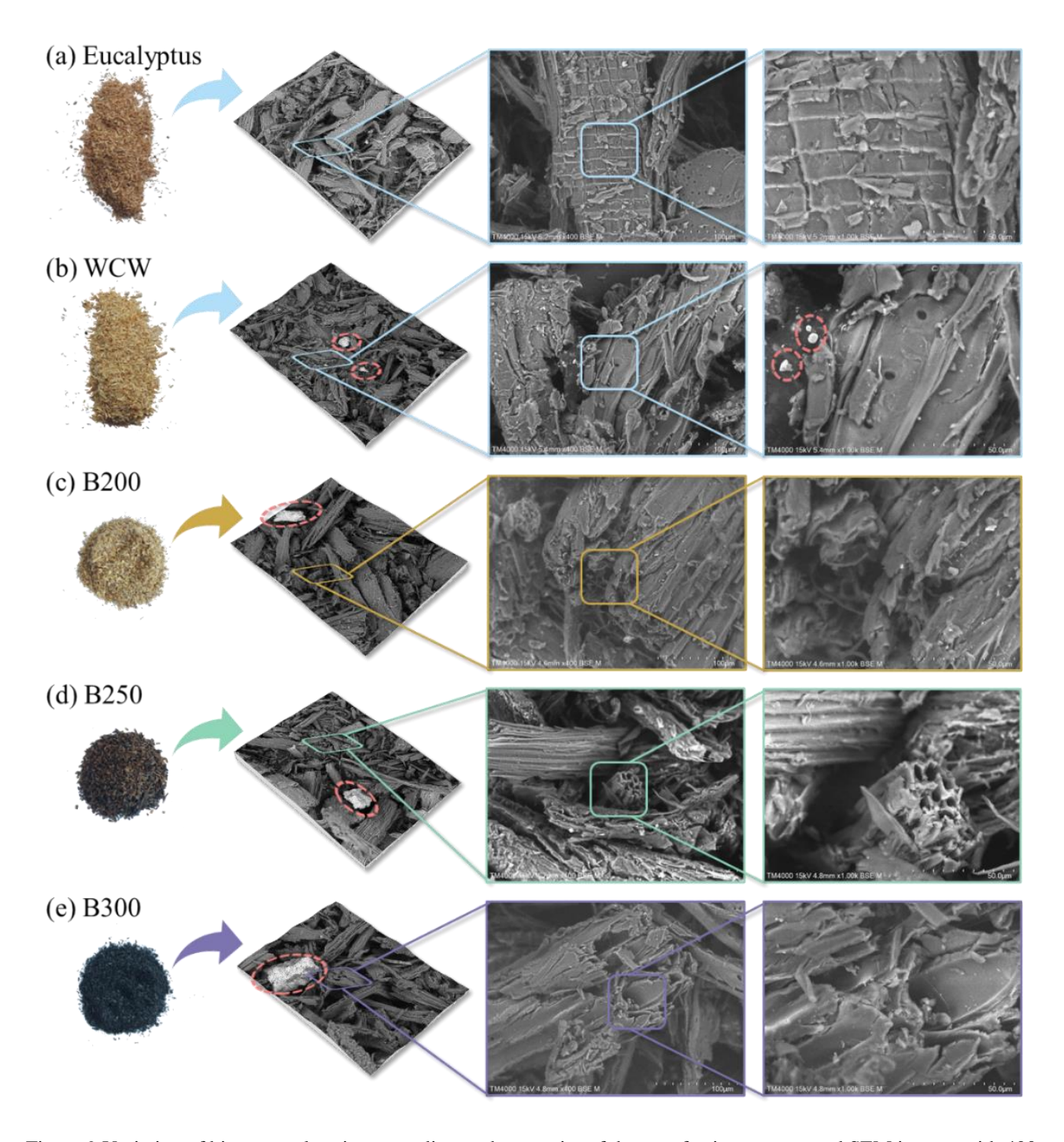


Figure 9. Variation of biomass coloration according to the severity of the torrefaction process and SEM images with 400 and 1000X for (a) raw *Eucalyptus* sp., (b) CWW, (c) B200, (d) B250, and (e) B300. Red circles indicated the contamination on CWW Source: Barbosa et al., (2024) [71]

# 4.3 TORREFACTION PERFORMANCE

# 4.3.1 Torrefaction Severity and Indexes

Figure (10) presents the calculated indexes (SY, TSI, and  $TSF_{dim}$  in Table 5) to assess the performance of torrefaction performances. Weight loss (WL) and Solid Yield (SY) are the primary indicators for assessing torrefaction severity [82]. It is commonly employed to evaluate the process, where higher severities (treatment temperatures and/or longer durations) lead to the decomposition of low-molecular-weight compounds (mainly hemicelluloses and part of cellulose and lignin) in the biomass, resulting in more significant weight loss (or lower SY) [82], [97], [99]. Therefore, the SY assesses the influence of operational conditions on solid biofuel production [83]. However, different biomasses possess an intrinsic degradation behavior dependency of torrefaction severity (light, mild, and severe) that must be assessed to characterize process performance.

TSI normalizes SY, allowing dimensionless comparison with other biomass samples and facilitating comparisons across different types. TSF improves SY information by highlighting biomass sensitivity to thermal degradation, enabling improved comparisons between different types, like hardwood and softwood.

The SY experimental curves were normalized after 160 °C since woody biomass degradation usually occurs for temperatures higher than 180 °C [102]. Accordingly, the mass loss at 160 °C was normalized to 100%. Figures 10 (a) and (b) illustrate the solid yield (SY) values for B200, B250, and B300, which are 98.44, 86.88, and 62.93%, respectively. As noted, light torrefaction (200 °C) did not affect the blend (with a slight 1.66% weight loss), and as the severity of the treatment increased, the treatment highly influenced the blend's thermal degradation. The blend degradation started at around 190 °C, aligned with *Eucalyptus* and Pine biomasses that reported thermal stability between 180–200 °C [134]. The obtained yield is in line with the SY of *Eucalyptus* (210–290 °C) and *Pine* torrefaction (250–290 °C with 60 min isothermal), which varied between 96.61–63.28% and 77.01–54.71%, respectively [98], [135].

By analyzing the 3D surfaces and contours of TSI (Fig. 10(c) and (f)) and  $TSF_{dim}$ , enables evaluating torrefaction performance and studying thermal degradation's dependence on time and temperature [82], [86], [136], [137]. The surface curvatures (Fig. 10(c) and (f)) illustrate that as the thermal degradation becomes increasingly sensitive to torrefaction severity (higher temperature and time), the curvatures become more pronounced [82]. As a result, the severity assessment can be based on temperature (intermediate curvature) and time (low and high curvatures) dependencies [82].

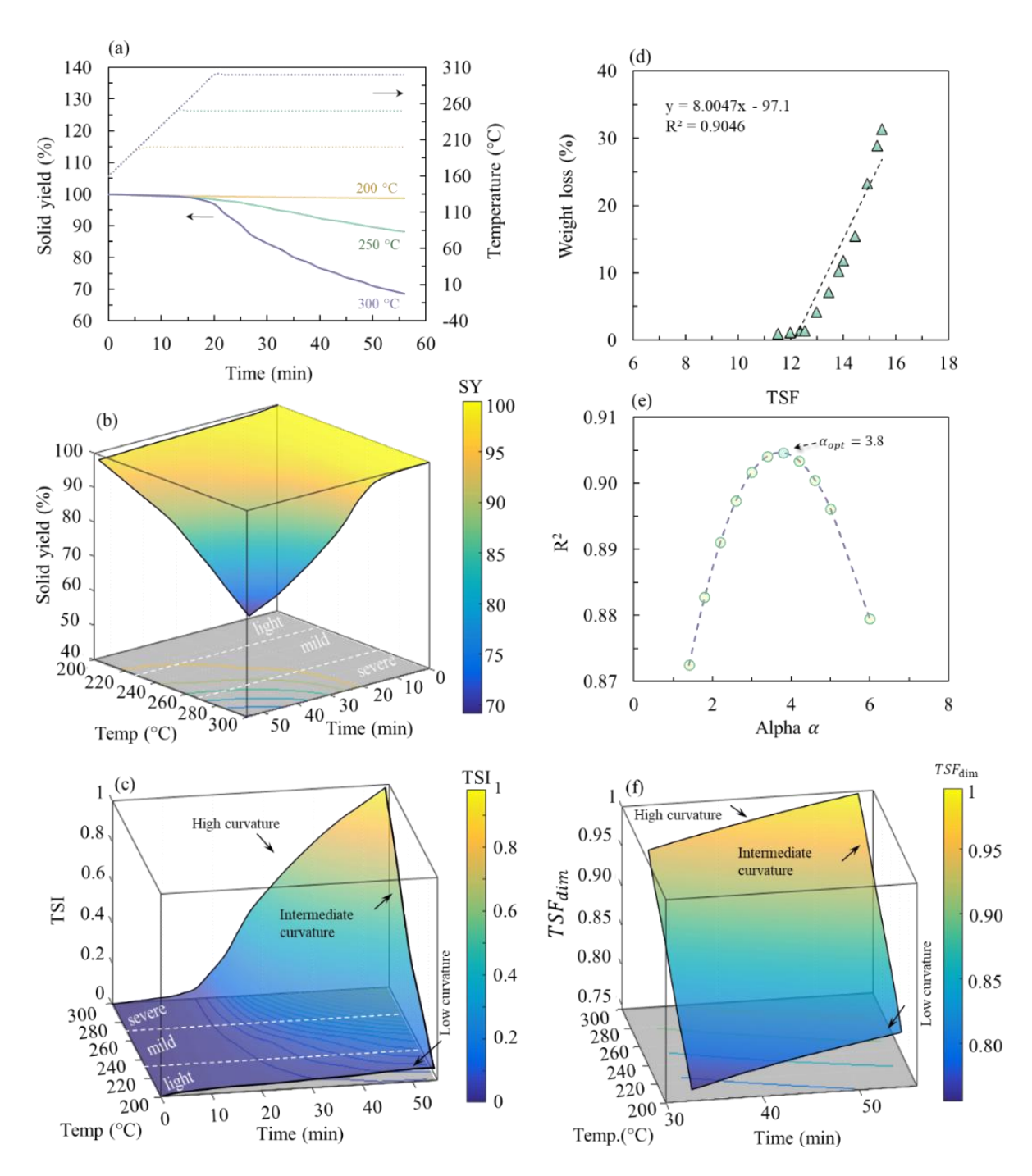


Figure 10. Experimental SY (%) and treatment temperature (°C) for torrefaction treatments. (b) Three-dimensional surface and two-dimensional contour mapping for the calculated SY as a function of treatment time and temperatures. (c) Three-dimensional surface and two-dimensional contour mapping for TSI as a function of treatment time and the reaction temperatures, highlighting the low, intermediate, and higher curvatures. White dashed lines indicate the transition from light to severe torrefaction. (d) Correlation between weight loss (%) and  $TSF_{dim}$  for optimum alpha value (3.8). (e) Profile of the coefficient of determination  $R^2$ . (f) Three-dimensional surface and two-dimensional contour mapping for  $TSF_{dim}$  highlighting the low, intermediate, and higher curvatures. Source: Barbosa et al., (2024) [71].

The low curvature of the TSI 3D surface exhibits a smooth degradation progression during

treatment, which implies a minor time dependence for lighter torrefaction. In contrast, the transition from light to mild torrefaction is marked by a notable time dependence, with the highest dependence observed for the most severe treatment (as indicated by the high curvature). This description accurately characterizes the torrefaction process, where mass loss gradients develop gradually and continuously at light torrefaction (200–235 °C), while more significant mass loss gradients are observed during severe treatments (275–300 °C).

As noted in Fig. 10 (c), after the heating period (first 12 min of treatment), the TSI evolution is faster in a shorter time, as depicted by the high curvature. This behavior can be interpreted by higher consumption and modification of biomass components (mainly hemicelluloses and cellulose), resulting in a faster volatile removal (dehydration reactions joint with the scission of weak linkages concerning small substituents and the leading polymer chains [138]) and, consequently, a torrefied product with enhanced coal-like properties.

As can be seen in Eq. 9 in Table 5, for calculating the  $TSF_{dim}$  it is required first to determine the optimum alpha  $(\alpha_{opt})$  value [86]. This determination of  $\alpha_{opt}$  is possible by varying the  $\alpha$  value on Eq. (9) and plotting the obtained  $TSF_{dim}$  and its related weight loss (for a specific torrefaction temperature  $(T_H)$ ), and when the coefficient of determination  $(R^2)$  of this linear fitting is maximized, the alpha optimum is defined [86]. This process is described in Fig. 10(d) and (f), which shows the linear correlation between the experimental mass loss and  $TSF_{dim}$  (for the maximum  $R^2 = 0.9046$  on Fig. 10(f)) and the process of varying the  $\alpha$  value to determine  $\alpha_{opt} = 3.8$ . Previous study on Eucalyptus grandis observed and  $\alpha = 2.7$  [82]. In addition, when investigating Chinese medicine residue, microalga Arthrospira platensis residue, microalga Chlamydomonas sp. JSC4 residue and spent coffee grounds, Chen et al. [86] reported  $\alpha$  values varying between 1.6–3. Moreover, an  $\alpha = 3.6$  was obtained for a blend composed of pruning tree residues [13]. The higher alpha value of 3.8 indicated a superior dependency of treatment time through torrefaction treatment.

Figure 10(f) depicts the 3D surface and accompanying 2D contour of  $TSF_{dim}$  obtained considering the  $\alpha_{opt}$ =3.8. Within this representation, the time and temperature dependencies through torrefaction treatment are discernible through the low, high, and intermediate curvatures [82]. As expected [13], the intermediate curvature has a linear behavior respected by  $TSF_{dim} = 0.002 \, \text{T}(^{\circ}\text{C}) + 0.4292$  and the final  $TSF_{dim}$  values for 200, 250, and 300 were 0.81, 0.90, and 1, respectively. In line with previous studies [13], [82], the low and high curvature have logarithm behavior presenting  $TSF_{dim} = 0.1066 \, \log(t) + 0.3805$  and  $TSF_{dim} = 0.1066 \, \log(t) + 0.5708$ 

reporting identical time dependence for both severities corroborated by the equal slope (0.1066), contrarily from the 3D surface of TSI that exhibited lower time dependency for lower (low curvature) than severe treatments (high curvature). Hence, TSI is more indicated for accounting for thermal degradation sensitivity to torrefaction severity than  $TSF_{dim}$ .

### 4.3.2 Torrefaction kinetics

The accuracy of the two-step reaction modeling approach was evident in the excellent agreement observed between the predicted curves and experimental data, as illustrated in Fig. 11. In addition, Table 8 presents the predicted values of the kinetic parameters, including pre-exponential factors and activation energies.

Table 8. Kinetic parameters (activation energy and pre-exponential factor) and curve fit quality (R<sup>2</sup>).

Reaction	Kinetic constant	$E_a i$	$A_oi$
$A \rightarrow B$	$k_1$	1.25E+02	7.76E+10
$A \rightarrow V_1$	$k_{V_1}$	1.13E+02	6.24E+08
$B \rightarrow C$	$k_2$	5.03E+01	7.76E+00
$B \rightarrow V_2$	$k_{V_2}$	1.04E+02	2.51E+07
Curve fit	200 °C	250 °C	300 °C
$R^2$	0.9860	0.9777	0.9944

 $\boldsymbol{E_a i}$ : Activation energy (kJ mol<sup>-1</sup>);  $\boldsymbol{A_o i}$ : pre-exponential factors (min<sup>-1</sup>), i=1,2,V<sub>1</sub> and V<sub>2</sub>

This proper alignment between the predicted curves and experimental data was also documented in previous studies that explored *Eucalyptus grandis* [98], urban forest wastes blend [13], *Miscanthus*, *Eucalyptus* and *Amapai* under catalytic conditions [100], and poplar [97], confirming the suitability of the chosen two-step reaction model for achieving favorable outcomes throughout the entire temperature range (200–300 °C) of torrefaction process. As a result, it offers high simulation accuracy and reasonable computation time across a wide range of parameters [78]. The curve fit demonstrated promising results with R<sup>2</sup> values of 0.9860, 0.9777, and 0.9944 for the 200, 250, and 300 °C torrefied blends, respectively. These high R<sup>2</sup> values indicate the effectiveness of the proposed model in accurately describing the mass loss prediction of a biomass blend consisting of CWW and *Eucalyptus*, which is essential for modeling torrefaction upscale.

The obtained kinetic constants  $(k_1, k_{V_1}, k_2, \text{ and } k_{V_2} \text{ in Table 8})$  are graphically displayed in the Arrhenius plot (Fig. 11(b)). The torrefaction process leads to a two-step degradation of hemicelluloses [97], therefore being correctly predicted by the two-step reaction model. Initially, glycosidic bonds are broken, and side chains decompose at approximately 233 °C. Subsequently,

monosaccharide units undergo fragmentation around 285 °C [139]. As noted in Fig. 11(b), the first-step reaction was faster than the second-step reaction  $(k_1 > k_{V_1} > k_2 > k_{V_2})$  for all torrefaction ranges in line with pure xylan torrefaction [89]. Therefore, indicating a faster first reaction step  $(A \rightarrow B \text{ and } A \rightarrow V_1)$  than the second  $(B \rightarrow C \text{ and } B \rightarrow V_2)$ . The increasing on torrefactions severity (temperature) showed faster kinetic constants, resulting in high degradation, in line with (Fig. 11). Results align with torrefaction kinetics of Norway forest residues [61].

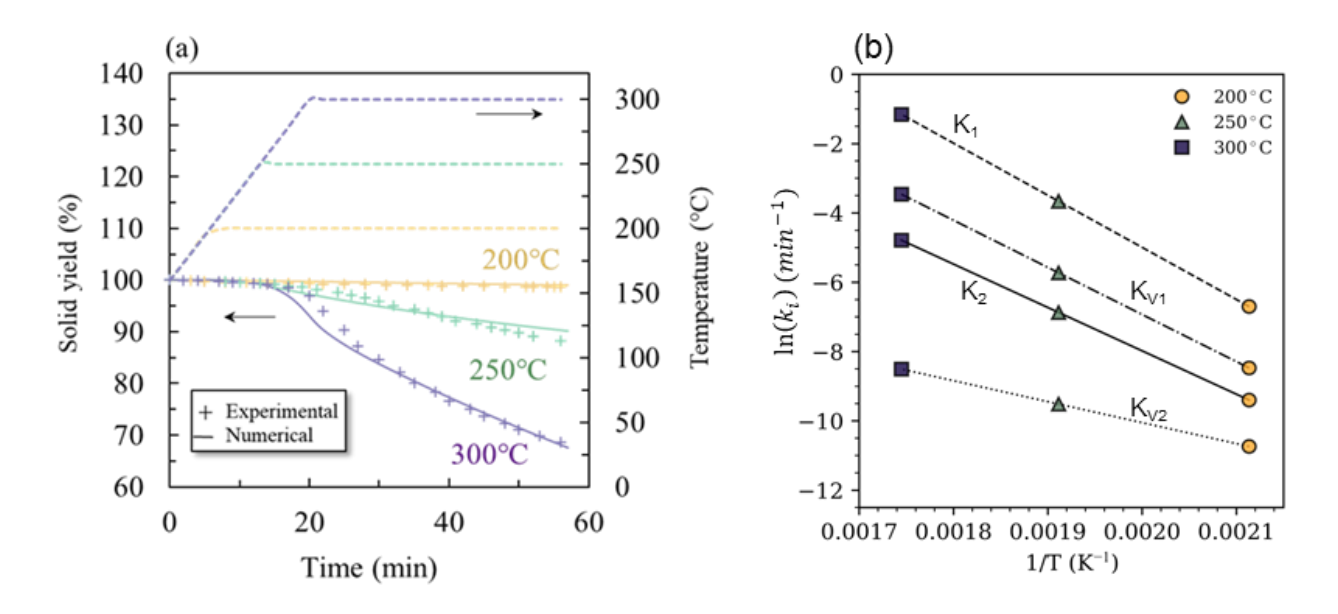


Figure 11. (a) Comparison between experimental (markers) and numerical (lines) SY. (b) Arrhenius plot: calculated reaction rates competition for 200–300 °C torrefied blends. Source: Barbosa et al., (2024) [71]

### 4.4 COMBUSTION BEHAVIOR

Figure 12 shows the thermogravimetric (a) and derivative curves for B (raw)(b), B200 (c), B250 (d), and B300 (e) combustion, allowing to assess the influence of torrefaction severity on the combustion behavior. In addition, Table 9 details the attributes associated with each decomposition stage, including the ignition temperature ( $T_i$ ), burnout temperature ( $T_f$ ), the maximum value of the 1<sup>st</sup> DTD peak (DTG<sub>max</sub>), and the temperature ( $T_{max}$ ) and time ( $t_{max}$ ) at which it occurred.

Several studies suggest that the most active element of biomass is hemicelluloses, which typically decomposes in the 220–280 °C range, while cellulose decomposes in the higher temperature range of 240–350 °C and lignin degrades slowly in the 250–500 °C range [69], [70]. Figure 12 shows that the primary oxidative (or combustion) reaction happens within 200–550 °C and reveals three

distinct phases related to the three upward peaks observed on the DTG curve. Thus, it aligns with the reported combustion behavior of other lignocellulosic biomass (*Eucalyptus* wood [132], [140], bamboo and sugarcane bagasse [141], polish wood [142], and rubberwood [143]).

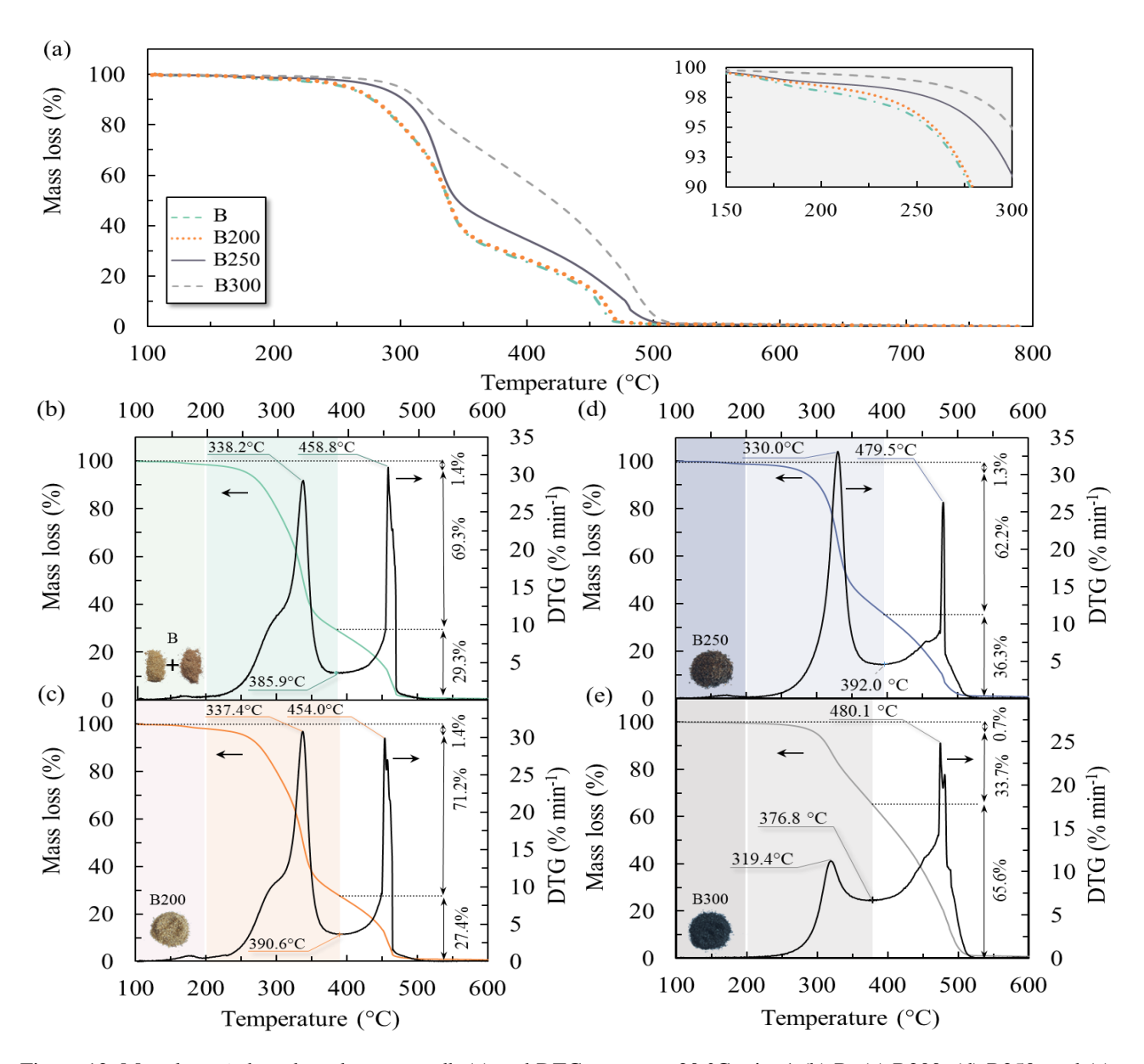


Figure 12. Mass loss %, based on dry mass - db (a) and DTG curves at  $20\,^{\circ}$ C min–1 (b) B, (c) B200, (d) B250, and (e) B300 combustion. Source: Barbosa et al., (2024) [71]

Since the TG curves were normalized at  $100\,^{\circ}$ C (after drying phases), the first phase revealed only a slight peak between  $100-200\,^{\circ}$ C, reporting a similar mass loss ( $\sim 1.4\%$ ) in TG curves below

200 °C for B (raw), B200 and B250 due to the release of moisture and light volatiles (which present similar volatilization temperature of moisture) [69]. B300 does not present a noticeable upward peak on the first phase with a 0.7% mass loss, indicating the conferred hydrophobicity of torrefied biomass [98].

Following the drying phase, a notable increase in the thermal stability of the torrefied product can be observed in Fig. 12(a), slightly differing for B200 and escalating with torrefaction severity (B250 and B300). Consequently, displacing the fuel's ignition and burnout temperatures towards higher temperatures, resulting in a shift of the 1<sup>st</sup> DTG peaks towards the higher temperature regions [109]. Raw blend (B) presented ignition and burnout temperatures of 232.36 and 472.82 °C, in line with raw *Eucalyptus* and Pine combustion behavior [132], [140], [144]. As expected [68], enhancements up to 269.9 and 515 °C (B300) on the ignition and burnout temperatures were evidenced, linked with reduced ignition and burnout index (Table 9). A superior  $D_i$  indicates a greater separation of volatile compounds from the fuel, facilitating smoother ignition [145]. Thus, the rise in  $T_i$  due to increased torrefaction severity naturally correlates with a decrease in  $D_i$  for torrefied products, aligning with findings from similar biomass residues [68].

The ignition performance is intrinsically related to ultimate and proximate properties. Initially, during combustion, B(raw) exhibited greater reactivity (lower  $T_i$ ) than torrefied products. In contrast to torrefied products, the raw material exhibits superior H/C and O/C ratios. This attribute reduces bonding energies due to carbon-oxygen bonds' lower energy than carbon-carbon bonds [106]. Consequently, the inherent characteristics of the raw material can prompt quicker ignition processes. Furthermore, this difference could be attributed to the raw feedstock's heightened VM (Table 7), which tends to lower  $T_i$ . Moreover, the heightened ash% within torrefied products confirms reduced ignition performance due to the influence of high ash amounts on oxygen diffusion and heat transfer [145].

Table 9. Combustion characteristic parameters of raw feedstock (B) and their torrefied products (B200, B250 and B300).

	Time (min)		Temperature (°C)			$DTG_{max}$	Indexes		
	$t_i$	$t_{max}$	$t_b$	$T_i$	$T_{max}$	$T_f$	(% min <sup>-1</sup> )	$D_i \times 10$	$D_f \times 10^3$
В	11.22	16.38	23.10	232.36	338.25	472.82	29.21	1.59	4.97
<b>B200</b>	11.37	16.31	23.17	235.60	337.39	473.12	30.77	1.66	5.22
B250	12.37	15.98	24.87	255.34	329.97	506.38	33.09	1.67	5.42
B300	13.07	15.41	25.28	269.94	319.41	515.02	11.25	0.56	1.97

 $D_i$  (% min<sup>-3</sup>),  $D_f$  (% min<sup>-4</sup>).

The second stage, attributed to cellulose and hemicelluloses decompositions, occurred between 200 °C and ~400 °C and reported a mass loss of approximately 69.3%, 71.2%, 62.2%, and 33.7% for B, B200, B250 and B300, respectively. Before the pronounced first peak, a characteristic shoulder appears on the DTG curve. This shoulder, clearly marked for B(raw) and B200 (Fig. 12(b) and (c)), is attributed mainly to the thermal degradation of hemicelluloses fraction, which is the most reactive part of biomass and typically decomposes in the range of 220–280 °C. The shoulder's shape decreases as the torrefaction severity increases (B250 and B300), indicating the decomposition of hemicelluloses through torrefaction.

Next, the thermal degradation of cellulose and the remaining part of hemicelluloses occurs between the temperature range of 240–350 °C, revealing a pronounced first peak.

Figure 12 shows evidence that torrefied products experience a reduction in the peak temperature ( $T_p$ ) and an elevation in  $DTG_{max}$  (B200 and B250) during combustion. The 1<sup>st</sup> DTG peaks were evident at temperatures 338.2, 337.4, 330.0, and 319.4 °C for B, B200, B250 and B300, respectively, in line with the combustion of torrefied urban forest waste [146]. Results also align with Lee et al. [147], which observed that pine samples show a decrease in peak temperature and an increase in  $DTG_{max}$  of oxidative pyrolysis and char combustion upon torrefaction, respectively. The severe treatment (B300) was characterized by the 1<sup>st</sup> DTG peak reduction, indicating an enhanced degradation of cellulose and hemicellulose through torrefaction.

The forthcoming phase (400–600 °C) is attributed partially to cellulose decomposition, as well as the lignin (whose degradation typically occurs over a more comprehensive temperature range [56]). This stage, characterized by the 2<sup>nd</sup> DTG peak, reflected a mass loss of around 29.3, 27.4, 36.3, and 65.67% and occurred at temperatures of 458.8, 454.0, 479.5 and 480.1 °C for B, B200, B250, and B300, respectively.

Finally (600–800 °C), a reduced mass loss was evidenced and can be attributed to the slow carbonization and degradation of the residual lignin, with a long tail stage accounting for 0.5% mass loss. Torrefied products produced under higher temperatures exhibited reduced ignition performance, rendering them more challenging to ignite and diminishing burnout efficiency [146]. In terms of  $T_f$ , the lower values observed in raw biomass suggest a diminished presence of unburnt substances. The analysis revealed that most thermal volatilization events in the blend sample, except B300, occur between 200 and 400 °C, accounting for more than 60% of total mass loss.

### 4.5 FOSSIL FUELS EQUIVALENCE AND CO<sub>2</sub> EMISSION MITIGATION

Table 10 displays the outcomes regarding the fossil fuel equivalence for 1 m<sup>3</sup> of biomass, encompassing both raw (B) and torrefied blends (B200, B250, and B300), along with Brazilian lignocellulosic wastes from the literature [110].

Table 10.Fossil fuel equivalence for 1 m3 of biomass and potential CO2 retention prevented by the valuation of CWW.

	Fossil fuels equivalence (L.m <sup>-3</sup> )				Potential CO <sub>2</sub> retention (kg CO <sub>2</sub> eq)			
	Petroleum	Diesel oil	Fuel oil	Gasoline	Petroleum	Diesel oil	Fuel oil	Gasoline
B (raw)	150.71	153.87	139.77	171.09	516.94	543.16	410.91	674.09
B200	159.96	163.32	148.35	181.59	548.67	576.50	436.14	715.46
<b>B250</b>	172.27	175.88	159.76	195.56	590.88	620.85	469.68	770.49
<b>B300</b>	154.34	157.57	143.13	175.20	529.37	556.22	420.79	690.29
Euca <sup>a</sup>	103.27	105.42	95.76	117.23	354.23	372.14	281.53	461.90
Pine <sup>a</sup>	92.04	93.95	85.34	104.48	315.68	331.64	25.89	411.63
RH <sup>a</sup>	91.73	93.63	85.05	104.13	314.63	330.53	250.06	410.26
CF a	119.10	121.57	110.43	135.2	408.51	429.15	324.67	532.67
SB <sup>a</sup>	48.61	49.62	45.07	55.18	166.72	175.15	132.51	217.4
BW <sup>a</sup>	74.94	76.5	69.49	85.07	257.05	270.04	204.29	335.18

<sup>&</sup>lt;sup>a</sup> Literature data from [110]. RH (Rice husk), CF (Coffee waste), SB (Sugarcane bagasse), BW (Bamboo waste).

The estimated fossil fuel equivalence for one cubic meter of torrefied blends ranges from 150.71 to 172.27 L.m<sup>-3</sup> of petroleum, 153.87 to 175.88 L.m<sup>-3</sup> of diesel oil, 139.77 to 159.76 L.m<sup>-3</sup> of fuel oil, and 171.09 to 195.56 L.m<sup>-3</sup> of gasoline. Compared to the literature on *Eucalyptus* and pine wastes from [110], the fossil fuel equivalence and, consequently, the CO<sub>2</sub> retention (kg CO<sub>2</sub> eq) were higher for B(raw) due to a higher bulk density of the proposed blend.

Given the inherent connection between fuel equivalence and the bioenergy index, B250 exhibited elevated fossil equivalences across all fuel types. This phenomenon stems from its heightened bulk density. In contrast to other biomass, the torrefied blends yield more significant fossil fuel volume equivalence, predominantly attributed to their superior bioenergy potential. Consequently, torrefaction emerges to enhance the applicability of CWW blends with *Eucalyptus*. For instance, a noteworthy 14.30% improvement in fossil fuel equivalence was achieved when comparing B250 to B(raw).

In the context of CO<sub>2</sub> emission reduction, Table 10 shows that the torrefied product showcases more potential than the raw blend and other lignocellulosic residues. To illustrate, replacing

petroleum, diesel oil, fuel oil, or gasoline with B250 as a biofuel could mitigate 590.88, 620.85, 469.68, and 770.49 kg CO<sub>2</sub>eq., respectively.

Pursuing new renewable materials is crucial for mitigating CO<sub>2</sub> emissions, particularly since coal is responsible for 44% of global fuel emissions [148]. Therefore, strategies and valuation routes such as torrefaction to enhance biomass residues' utilization for energy generation are paramount.

In a prior study by Roy et al. (2009) [149], predictive equations were introduced to estimate carbon dioxide emissions per unit of coal mass and energy consumption, presenting a reliable method for evaluating coal combustion emissions. Their findings, focusing on coking coal (steel grade I), indicated emissions ranging from 90 to 97 t CO<sub>2</sub> TJ<sup>-1</sup>. Regarding B200, B250 and B300, the torrefaction treatment yielded an LHV of 18.71, 19.53 and 23.18 MJ kg<sup>-1</sup>, respectively. Therefore, substituting 1 t of mineral coal with the proposed blend torrefied at 200, 250 and 300 °C would avoid emitting 1683.9–1762.6, 1757.7–1894.4 and 2086.2–2248.46 kg CO<sub>2</sub>, respectively.

### 5 LIMITATIONS AND PROSPECTS

Future research should consider the potential variations in the chemical composition of CWW, particularly in terms of ash content. These residues exhibit considerable variability and may contain varying proportions of contaminants. The increased ash content may potentially have adverse effects on combustion equipment. Therefore, it is recommended that the inorganic composition of ash and ash melting behavior be investigated to consider issues related to fouling, deposition, and slag formation in combustion equipment. In addition, synergistic effects may occur during the thermal upgrading of biomass blends during ash formation, which can impact the results (and the performance of biomass during combustion). Future studies are recommended to assess these effects.

It is worth noting in the text that the 50:50 blend was chosen for operational ease, implying that entrepreneurs and researchers can replicate the results obtained in this study on an operational scale (such as in biomass compaction and torrefaction industries). Future research will contemplate optimization techniques (Response surface methodology [121] and multicriteria decision analysis [150], [151]) to determine the ideal proportion of each biomass for producing a superior biofuel with lower ash content.

Another point of interest is the benefits associated with transportation logistics and emissions reduction, which could be achieved with mechanical treatments for densification such as palletization [50] and briquetting [68]. Planning the supply chain for a specific enterprise or energy system and evaluating the mitigation of diesel emissions during transportation could be considered within the life cycle assessment.

# 6 CONCLUSION

This research demonstrates progress in utilizing CWW as a biofuel through torrefaction, addressing torrefaction kinetics, combustion behavior, and potential CO<sub>2</sub> retention. Blending CWW with other biomass emerges as a viable strategy to optimize its utilization while minimizing ash content, addressing concerns of boilers corrosion and slag formation during combustion. The biomass studied is produced in substantial quantities in Brazil, offering a promising avenue to integrate waste into the country's energy matrix in alignment with SDGs.

Key outcomes highlight the efficacy of treatment B250, with 1.24% ash, HHV of 20.76 MJ kg<sup>-1</sup>, mass yield of 86.88%, energy yield of 91.25%, and bioenergy index of 6.38 GJm<sup>-3</sup>. B300 exhibits properties akin to fossil fuels but with lower energy and gravimetric yields. Notably, B200 and B250 show a significant increase in bioenergy index, indicating their potential for energy generation.

Results underscores insights for replacing traditional fuels with a torrefied blend, offering a practical avenue for reducing CO<sub>2</sub>eq emissions, representing an environmentally friendly alternative, promoting waste reuse, and mitigating environmental impacts.

### **BIBLIOGRAPHIC REFERENCES**

- [1] L. P. Thives, E. Ghisi, and J. J. Thives Júnior, "An outlook on the management of construction and demolition waste in Brazil," *Clean. Mater.*, vol. 6, no. September, p. 100153, 2022, doi: 10.1016/j.clema.2022.100153.
- [2] M. Edo, N. Skoglund, Q. Gao, P. E. Persson, and S. Jansson, "Fate of metals and emissions of organic pollutants from torrefaction of waste wood, MSW, and RDF," *Waste Manag.*, vol. 68, pp. 646–652, 2017, doi: 10.1016/j.wasman.2017.06.017.
- [3] W. H. Chen, J. Peng, and X. T. Bi, "A state-of-the-art review of biomass torrefaction, densification and applications," *Renew. Sustain. Energy Rev.*, vol. 44, pp. 847–866, 2015, doi: 10.1016/j.rser.2014.12.039.
- [4] M. Ivanovski, D. Goricanec, J. Krope, and D. Urbancl, "Torrefaction pretreatment of lignocellulosic biomass for sustainable solid biofuel production," *Energy*, vol. 240, p. 122483, 2022, doi: 10.1016/j.energy.2021.122483.
- [5] W. H. Chen and P. C. Kuo, "A study on torrefaction of various biomass materials and its impact on lignocellulosic structure simulated by a thermogravimetry," *Energy*, vol. 35, no. 6, pp. 2580–2586, 2010, doi: 10.1016/j.energy.2010.02.054.
- [6] E. A. Silveira *et al.*, "Biofuel from agro-industrial residues as sustainable strategy for CO2 mitigation: Statistical optimization of pequi seeds torrefaction," *Energy Convers. Manag.*, vol. 304, no. November 2023, 2024, doi: 10.1016/j.enconman.2024.118222.
- [7] N. Tamires da Silva Carvalho, E. A. Silveira, T. de Paula Protásio, P. F. Trugilho, and M. L. Bianchi, "Hydrotreatment of Eucalyptus sawdust: The influence of process temperature and H2SO4 catalyst on hydrochar quality, combustion behavior and related emissions," *Fuel*, vol. 360, no. November 2023, 2024, doi: 10.1016/j.fuel.2023.130643.
- [8] T. R. Sarker, S. Nanda, A. K. Dalai, and V. Meda, "A Review of Torrefaction Technology for Upgrading Lignocellulosic Biomass to Solid Biofuels," *Bioenergy Res.*, vol. 14, no. 2, pp. 645–669, 2021, doi: 10.1007/s12155-020-10236-2.
- [9] M. Cozier, "Business highlights: Collaboration: Bigger and beta," *Biofuels, Bioprod. Biorefining*, vol. 8, no. 6, p. 743, 2014, doi: 10.1002/BBB.
- [10] W. H. Chen *et al.*, "Progress in biomass torrefaction: Principles, applications and challenges," *Prog. Energy Combust. Sci.*, vol. 82, 2021, doi:

- 10.1016/j.pecs.2020.100887.
- [11] United Nations, "UN General Assembly, Transforming our world: The 2030 agenda for sustainable development," Resolut. Adopt. by Gen. Assem. 25 Sept. 2015, vol. 16301, no. October, pp. 1–35, 2015, [Online]. Available: https://www.refworld.org/docid/57b6e3e44.html
- [12] M. Mahdavi, K. Schmitt, R. A. V. Ramos, and H. H. Alhelou, "Role of hydrocarbons and renewable energies in Iran's energy matrix focusing on bioenergy: review," *IET Renew. Power Gener.*, vol. 16, no. 15, pp. 3384–3405, 2022, doi: 10.1049/rpg2.12540.
- [13] E. A. Silveira *et al.*, "Urban lignocellulosic waste as biofuel: thermal improvement and torrefaction kinetics," *J. Therm. Anal. Calorim.*, vol. 148, no. 1, pp. 197–212, 2023, doi: 10.1007/s10973-022-11515-0.
- [14] C. M. Grottola, P. Giudicianni, J. B. Michel, and R. Ragucci, "Torrefaction of Woody Waste for Use as Biofuel," *Energy and Fuels*, vol. 32, no. 10, pp. 10266–10271, 2018, doi: 10.1021/acs.energyfuels.8b01136.
- [15] C. R. Andrade, J. O. Brito, A. F. Dias Junior, and A. Q. Lana, "Changes caused by torrefaction on urban wooden waste," pp. 275–284, 2017.
- [16] K. L. Iroba, O. D. Baik, and L. G. Tabil, "Torrefaction of biomass from municipal solid waste fractions I: Temperature profiles, moisture content, energy consumption, mass yield, and thermochemical properties," *Biomass and Bioenergy*, vol. 105, pp. 320– 330, 2017, doi: 10.1016/j.biombioe.2017.07.009.
- [17] K. L. Iroba, O. D. Baik, and L. G. Tabil, "Torrefaction of biomass from municipal solid waste fractions II: Grindability characteristics, higher heating value, pelletability and moisture adsorption," *Biomass and Bioenergy*, vol. 106, pp. 8–20, 2017, doi: 10.1016/j.biombioe.2017.08.008.
- [18] A. C. O. Fiorini *et al.*, "How climate change is impacting the Brazilian agricultural sector: evidence from a systematic literature review," *Environ. Res. Lett.*, vol. 19, no. 8, 2024, doi: 10.1088/1748-9326/ad5f42.
- [19] J. Sillmann *et al.*, "Climate extremes and risks: links between climate science and decision-making," *Front. Clim.*, vol. 6, no. December, pp. 1–12, 2024, doi: 10.3389/fclim.2024.1499765.
- [20] S. de E. de E. e R. de G. de E. E. SEEG, "Análise das emissões de efeito gases estufa

- e suas implicações para as metas climáticas do Brasil 1970-2023," 2024, [Online]. Available: https://oc.eco.br/wp-content/uploads/2024/11/FINAL\_SEEG\_emissoes\_2024\_v7.pdf?form=MG0AV3&for m=MG0AV3
- [21] BRASIL, "Balanço Energético Nacional (BEN) Relatório Síntese 2024, Ano base 2023," *Empres. Pesqui. Energética*, pp. 1–71, 2024.
- [22] C. N. da I. CNI, "Descarbonização da indústria Análise de experiências internacionais e recomendações para o Brasil," 2024. [Online]. Available: https://bit.ly/4hywkGa?r=qr
- [23] C. B. da I. da C. C. CBIC, "Desempenho da Construção Civil em 2024 e perspectivas para 2025," p. 28, 2024, [Online]. Available: https://cbic.org.br/wp-content/uploads/2020/12/balanco-construcao-2020-2021.pdf
- [24] J. S. ALTSCHUL, I. P. V. de OLIVEIRA, and M. de J. R. da NÓBREGA, "Resíduo Da Construção E Demolição Tecnologias E Problemas: Um Estudo De Caso," *Rev. Tecnológica da Univ. St. Úrsula*, vol. 3, no. 1, pp. 13–31, 2020, [Online]. Available: http://revistas.icesp.br/index.php/TEC-USU/article/view/1202
- [25] A. B. de R. e M. A. ABREMA, "Panorama dos resíduos sólidos no Brasil 2024.," pp. 1–23, 2024, [Online]. Available: https://www.abrema.org.br/panorama/
- [26] BRASIL, *Lei nº 12.305, de 2 de agosto de 2010. Institui a Política Nacional de Resíduos Sólidos e dá outras providências.* Diário Oficial da República Federativa do Brasil, Brasília, DF, 3 ago. 2010, 2010. [Online]. Available: http://www.planalto.gov.br/ccivil\_03/\_ato2007-2010/2010/lei/l12305.htm
- [27] C. N. D. M. A. Conama, "Resolução nº 307 do Conselho Nacional do Meio Ambiente, de 2002," pp. 3–6, 2002, [Online]. Available: http://www.mma.gov.br/port/conama/legislacao/CONAMA\_RES\_CONS\_1989\_005.p df
- [28] J. A. PASCHOALIN FILHO, "O setor da construção e a geração de resíduos: A necessidade de discussão de um novo paradigma."
- [29] K. da S. Cunha, J. C. A. Roberto, S. P. Souto, and S. C. Lima, "Resíduos sólidos na construção civil no Brasil," Rev. Gestão e Secr. (Management Adm. Prof. Rev., vol. 14, no. 6, pp. 8671–8692, 2023, doi: 10.7769/gesec.v14i6.2255.
- [30] C. C. Maestrello, "Reaproveitamento de resíduos de madeira da construção civil para geração de energia revisão," *CONSTRUINDO*, vol. v. 13, n., 2021.

- [31] N. E. G. S. S. M. G. de O. S. F. B. C. do N. G. S. da Silva, "RESÍDUOS DE MADEIRA PRODUZIDOS NA CONSTRUÇÃO CIVIL," pp. 207–214, 2016.
- [32] J. M. Reis, "Diagnóstico dos resíduos de construção e demolição coletados no município de Lavras-MG: um estudo para a implementação de uma usina de triagem e reciclagem.," 2021.
- [33] A. R. L. Ferreira and H. C. Moreira, "Critical Analysis of the Construction Waste Management: Case Study of the City of Rio de Janeiro (in Portuguese).," p. 136, 2013.
- [34] L. Fagundes and R. Miranda, "A reciclagem de residuos de construção e demolição no Brasil: 1986-2008," *Ambient. Constrúido*, pp. 57–71, 2009.
- [35] J. da C. M. Neto and V. Schalch, "Diagnóstico para estudo de gestão dos resíduos de construção e demolição do município de São Carlos," 2003.
- [36] F. da S. Souza, "Reinserção do resíduo de construção e demolição na cadeia produtiva da construção civil em Rio Branco-Acre.," pp. 6–8, 2021.
- [37] A. C. Bertol, A. Raffler, and J. P. Dos Santos, "Análise da correlação entre a geração de resíduos da construção civil e as características das obras," p. 77, 2013.
- [38] B. S. Schuster and L. R. Taboni Junior, "Práticas Aplicadas No Canteiro De Obras Que Contribuem Para a Gestão Sustentável Dos Resíduos Da Construção Civil," *Rev. Gestão Sustentabilidade Ambient.*, vol. 9, p. 781, 2020, doi: 10.19177/rgsa.v9e02020781-799.
- [39] F. P. Lopes, P. M. Pereira, and R. M. Hamaya, "Análise da contaminação em resíduos de madeira na construção civil," 2013.
- [40] M. Rivera-Tenorio and R. Moya, "Potential for pellet manufacturing with wood waste from construction in Costa Rica," *Waste Manag. Res.*, vol. 38, no. 8, pp. 886–895, 2020, doi: 10.1177/0734242X19893022.
- [41] G. Kiesnere, D. Atstaja, N. Cudecka-Purina, and R. Susniene, "The Potential of Wood Construction Waste Circularity," *Environ. MDPI*, vol. 11, no. 11, 2024, doi: 10.3390/environments11110231.
- [42] L. P. Rosado, "Avaliação do Ciclo de Vida de Alternativas para o Gerenciamento Integrado de Resíduos da Construção Civil do Município de Limeira/SP, Brasil.," *Univ. Estadual Campinas*, p. 345, 2015.
- [43] C. S. Poon, A. T. W. Yu, and L. H. Ng, "On-site sorting of construction and demolition waste in Hong Kong," *Resour. Conserv. Recycl.*, vol. 32, no. 2, pp. 157–172, 2001,

- doi: 10.1016/S0921-3449(01)00052-0.
- [44] W. M. Cavalcanti and E. J. Alves, "Aplicação De Resíduos Da Construção Civil Como Aglomerado De Compósitos De Madeira Péletes / Briquetes : Um Estudo Bibliográfico E Documental," *Congr. Sul Am. Resíduos Sólidos e Sustentabilidade*, no. June, pp. 1–8, 2018.
- [45] Sri Shalini S, Palanivelu K, Ramachandran A, and V. Raghavan, "Biochar from biomass waste as a renewable carbon material for climate change mitigation in reducing greenhouse gas emissions—a review," *Biomass Convers. Biorefinery*, vol. 11, no. 5, pp. 2247–2267, 2021, doi: 10.1007/s13399-020-00604-5.
- [46] T. X. Xd, D. X. Xd, and D. X. Xd, "Lignocellulosic biomass pyrolysis mechanism: A state-of-the-art review," *Prog. Energy Combust. Sci.*, vol. 62, pp. 33–86, 2017, doi: 10.1016/j.pecs.2017.05.004.
- [47] P. Basu, "Biomass Gasification, Pyrolysis and Torrefaction Practical Design and Theory," *Biomass Gasif. Des. Handb.*, pp. 65–96, 2010, doi: 10.1016/b978-0-12-374988-8.00003-9.
- [48] T. A. Mamvura and G. Danha, "Biomass torrefaction as an emerging technology to aid in energy production," *Heliyon*, vol. 6, no. 3, p. e03531, 2020, doi: 10.1016/j.heliyon.2020.e03531.
- [49] W. A. Kenney, L. Sennerby-Forsse, and P. Layton, "A review of biomass quality research relevant to the use of poplar and willow for energy conversion," *Biomass*, vol. 21, no. 3, pp. 163–188, 1990, doi: 10.1016/0144-4565(90)90063-P.
- [50] D. Nhuchhen, P. Basu, and B. Acharya, "A Comprehensive Review on Biomass Torrefaction," *Int. J. Renew. Energy Biofuels*, vol. 2014, pp. 1–56, 2014, doi: 10.5171/2014.506376.
- [51] J. Peng, X. T. Bi, J. Lim, and S. Sokhansanj, "Development of torrefaction kinetics for British Columbia softwoods," *Int. J. Chem. React. Eng.*, vol. 10, no. 1, 2012, doi: 10.1515/1542-6580.2878.
- [52] W.-H. Chen *et al.*, "Progress in biomass torrefaction: Principles, applications and challenges," *Prog. Energy Combust. Sci.*, vol. 82, p. 100887, Jan. 2021, doi: 10.1016/j.pecs.2020.100887.
- [53] W. H. Chen and P. C. Kuo, "Torrefaction and co-torrefaction characterization of hemicellulose, cellulose and lignin as well as torrefaction of some basic constituents

- in biomass," *Energy*, vol. 36, no. 2, pp. 803–811, 2011, doi: 10.1016/j.energy.2010.12.036.
- [54] D. Chen, A. Gao, K. Cen, J. Zhang, X. Cao, and Z. Ma, "Investigation of biomass torrefaction based on three major components: Hemicellulose, cellulose, and lignin," *Energy Convers. Manag.*, vol. 169, no. April, pp. 228–237, 2018, doi: 10.1016/j.enconman.2018.05.063.
- [55] W. H. Chen, P. C. Kuo, S. H. Liu, and W. Wu, "Thermal characterization of oil palm fiber and eucalyptus in torrefaction," *Energy*, vol. 71, pp. 40–48, 2014, doi: 10.1016/j.energy.2014.03.117.
- [56] H. Yang, R. Yan, H. Chen, D. H. Lee, and C. Zheng, "Characteristics of hemicellulose, cellulose and lignin pyrolysis," *Fuel*, vol. 86, no. 12–13, pp. 1781–1788, Aug. 2007, doi: 10.1016/j.fuel.2006.12.013.
- [57] S. Ren, H. Lei, L. Wang, Q. Bu, S. Chen, and J. Wu, "Thermal behaviour and kinetic study for woody biomass torrefaction and torrefied biomass pyrolysis by TGA," *Biosyst. Eng.*, vol. 116, no. 4, pp. 420–426, 2013, doi: 10.1016/j.biosystemseng.2013.10.003.
- [58] M. J. Prins, K. J. Ptasinski, and F. J. J. G. J. G. Janssen, "Torrefaction of wood. Part 1. Weight loss kinetics," *J. Anal. Appl. Pyrolysis*, vol. 77, no. 1, pp. 28–34, 2006, doi: 10.1016/j.jaap.2006.01.002.
- [59] M. J. Prins, K. J. Ptasinski, and F. J. J. G. Janssen, "Torrefaction of wood. Part 2. Analysis of products," *J. Anal. Appl. Pyrolysis*, vol. 77, no. 1, pp. 35–40, 2006, doi: 10.1016/j.jaap.2006.01.001.
- [60] R. B. Bates and A. F. Ghoniem, "Biomass torrefaction: Modeling of volatile and solid product evolution kinetics," *Bioresour. Technol.*, vol. 124, pp. 460–469, 2012, doi: 10.1016/j.biortech.2012.07.018.
- [61] Q. V. Bach, W. H. Chen, Y. S. Chu, Ø. Skreiberg, ??yvind Skreiberg, and Ø. Skreiberg, "Predictions of biochar yield and elemental composition during torrefaction of forest residues," *Bioresour. Technol.*, vol. 215, pp. 239–246, 2016, doi: 10.1016/j.biortech.2016.04.009.
- [62] J. J. Chew, V. Doshi, S. T. Yong, and S. Bhattacharya, "Kinetic study of torrefaction of oil palm shell, mesocarp and empty fruit bunch," *J. Therm. Anal. Calorim.*, vol. 126, no. 2, pp. 709–715, 2016, doi: 10.1007/s10973-016-5518-3.

- [63] P. C. a Bergman, a R. Boersma, R. W. R. Zwart, and J. H. a Kiel, "Torrefaction for biomass co-firing in existing coal-fired power stations," *Energy Res. Cent. Netherlands ECN ECNC05013*, no. July, p. 71, 2005, [Online]. Available: http://www.ecn.nl/publications/PdfFetch.aspx?nr=ECN-C--05-013
- [64] L. Shang *et al.*, "Intrinsic kinetics and devolatilization of wheat straw during torrefaction," *J. Anal. Appl. Pyrolysis*, vol. 100, pp. 145–152, 2013, doi: 10.1016/j.jaap.2012.12.010.
- [65] M. O. Dos Santos Silva et al., "Thermogravimetric characteristics and combustion of Tachigali vulgaris wood planted at different spacings," Sci. For. Sci., vol. 49, no. 129, 2021, doi: 10.18671/SCIFOR.V49N129.01.
- [66] S. S. Idris, N. A. Rahman, and K. Ismail, "Combustion characteristics of Malaysian oil palm biomass, sub-bituminous coal and their respective blends via thermogravimetric analysis (TGA)," *Bioresour. Technol.*, vol. 123, no. 2012, pp. 581–591, 2012, doi: 10.1016/j.biortech.2012.07.065.
- [67] V. Leroy, D. Cancellieri, and E. Leoni, "Thermal degradation of ligno-cellulosic fuels: DSC and TGA studies," *Thermochim. Acta*, vol. 451, no. 1–2, pp. 131–138, 2006, doi: 10.1016/j.tca.2006.09.017.
- [68] B. S. Chaves *et al.*, "Production and characterization of raw and torrefied phyllostachys aurea pellets and briquettes for energy purposes," in *29th European Biomass Conference and Exhibition*, 2021, pp. 657–661. doi: 10.5071/29thEUBCE2021-2DV.2.1.
- [69] P. Brachi, F. Miccio, M. Miccio, and G. Ruoppolo, "Isoconversional kinetic analysis of olive pomace decomposition under torrefaction operating conditions," *Fuel Process. Technol.*, vol. 130, no. C, pp. 147–154, 2015, doi: 10.1016/j.fuproc.2014.09.043.
- [70] J. S. Tumuluru, S. Sokhansanj, J. R. Hess, C. T. Wright, and R. D. Boardman, "A review on biomass torrefaction process and product properties for energy applications," *Ind. Biotechnol.*, vol. 7, no. 5, pp. 384–401, 2011, doi: 10.1089/ind.2011.0014.
- [71] T. Barbosa *et al.*, "Waste-to-energy in the civil-construction sector toward the valuation of wood construction residues: Integration of torrefaction process," *Fuel*, vol. 371, Sep. 2024, doi: 10.1016/j.fuel.2024.132029.
- [72] T. Barbosa et al., "Torrefaction of Wood Construction Waste and Eucalyptus Blends

- for Biofuel With Enhanced Energy Density and Low Ash Content," *Eur. Biomass Conf. Exhib. Proc.*, no. June, pp. 157–163, 2023.
- [73] T. Barbosa, "Torrefação de blendas de madeira de construção e resíduos lignocelulósicos para uso energético," 2022. [Online]. Available: http://scioteca.caf.com/bitstream/handle/123456789/1091/RED2017-Eng-8ene.pdf?sequence=12&isAllowed=y%0Ahttp://dx.doi.org/10.1016/j.regsciurbeco.20 08.06.005%0Ahttps://www.researchgate.net/publication/305320484\_SISTEM\_PEM BETUNGAN\_TERPUSAT\_STRATEGI\_MELESTARI
- [74] A. F. Dias Junior *et al.*, "Investigating the pyrolysis temperature to define the use of charcoal," *Eur. J. Wood Wood Prod.*, vol. 78, no. 1, pp. 193–204, 2020, doi: 10.1007/s00107-019-01489-6.
- [75] R. B. W. Evaristo *et al.*, "Multiparameter-analysis of CO2/Steam-enhanced gasification and pyrolysis for syngas and biochar production from low-cost feedstock," *Energy Convers. Manag. X*, vol. 12, p. 100138, Dec. 2021, doi: 10.1016/j.ecmx.2021.100138.
- [76] L. N. B. Menezes *et al.*, "Alternative valuation pathways for primary, secondary, and tertiary sewage sludge: biochar and bio-oil production for sustainable energy," *Biomass Convers. Biorefinery*, Apr. 2022, doi: 10.1007/s13399-022-02543-9.
- [77] M. S. Santanna, E. A. Silveira, L. Macedo, L. G. O. Galvão, and A. Caldeira-Pires, "Torrefaction of lignocellulosic municipal solid waste: Thermal upgrade for energy use," *Eur. Biomass Conf. Exhib. Proc.*, no. September, pp. 188–191, 2020, doi: 10.5071/28thEUBCE2020-1DV.1.34.
- [78] W. H. Chen, K. M. Lu, W. J. Lee, S. H. Liu, and T. C. Lin, "Non-oxidative and oxidative torrefaction characterization and SEM observations of fibrous and ligneous biomass," Appl. Energy, vol. 114, pp. 104–113, 2014, doi: 10.1016/j.apenergy.2013.09.045.
- [79] B. J. Lin *et al.*, "An evaluation of thermal characteristics of bacterium Actinobacillus succinogenes for energy use and circular bioeconomy," *Bioresour. Technol.*, vol. 301, no. December 2019, p. 122774, 2020, doi: 10.1016/j.biortech.2020.122774.
- [80] W. H. Chen, M. Y. Huang, J. S. Chang, C. Y. Chen, and W. J. Lee, "An energy analysis of torrefaction for upgrading microalga residue as a solid fuel," *Bioresour. Technol.*, vol. 185, pp. 285–293, 2015, doi: 10.1016/j.biortech.2015.02.095.
- [81] C. Zhang, S. H. Ho, W. H. Chen, Y. Xie, Z. Liu, and J. S. Chang, "Torrefaction

- performance and energy usage of biomass wastes and their correlations with torrefaction severity index," *Appl. Energy*, vol. 220, no. September 2017, pp. 598–604, 2018, doi: 10.1016/j.apenergy.2018.03.129.
- [82] E. A. Silveira, S. Luz, K. Candelier, L. A. Macedo, and P. Rousset, "An assessment of biomass torrefaction severity indexes," *Fuel*, vol. 288, p. 119631, Mar. 2021, doi: 10.1016/j.fuel.2020.119631.
- [83] E. A. Silveira *et al.*, "Effect of torrefaction on thermal behavior and fuel properties of Eucalyptus grandis macro-particulates," *J. Therm. Anal. Calorim.*, vol. 138, no. 5, pp. 3645–3652, Dec. 2019, doi: 10.1007/s10973-018-07999-4.
- [84] P. Basu, A. Kulshreshtha, and B. Acharya, "An Index for Quantifying the Degree of Torrefaction," *BioResources*, vol. 12, no. 1, pp. 1749–1766, 2017, doi: 10.15376/biores.12.1.1749-1766.
- [85] K. S. Kung, S. K. Thengane, and A. F. Ghoniem, "Functional mapping of torrefied product characteristics with index of torrefaction," *Fuel Process. Technol.*, vol. 202, no. December 2019, p. 106362, 2020, doi: 10.1016/j.fuproc.2020.106362.
- [86] W. H. Chen, C. L. Cheng, P. L. Show, and H. C. Ong, "Torrefaction performance prediction approached by torrefaction severity factor," *Fuel*, vol. 251, no. January, pp. 126–135, 2019, doi: 10.1016/j.fuel.2019.04.047.
- [87] W. H. Chen and R. Aniza, "Specific chemical bioexergy and microwave-assisted torrefaction optimization via statistical and artificial intelligence approaches," *Fuel*, vol. 333, no. P2, p. 126524, 2023, doi: 10.1016/j.fuel.2022.126524.
- [88] G. Song, L. Shen, and J. Xiao, "Estimating specific chemical exergy of biomass from basic analysis data," *Ind. Eng. Chem. Res.*, vol. 50, no. 16, pp. 9758–9766, 2011, doi: 10.1021/ie200534n.
- [89] C. Di Blasi and M. Lanzetta, "Intrinsic kinetics of isothermal xylan degradation in inert atmosphere," *J. Anal. Appl. Pyrolysis*, vol. 40–41, pp. 287–303, May 1997, doi: 10.1016/S0165-2370(97)00028-4.
- [90] Q. Nguyen, D. D. Nguyen, H. Vothi, C. He, M. Goodarzi, and Q. V. Bach, "Isothermal torrefaction kinetics for sewage sludge pretreatment," *Fuel*, vol. 277, no. April, p. 118103, 2020, doi: 10.1016/j.fuel.2020.118103.
- [91] S. Gul, N. Ramzan, M. A. Hanif, and S. Bano, "Kinetic, volatile release modeling and optimization of torrefaction," *J. Anal. Appl. Pyrolysis*, vol. 128, no. May, pp. 44–53,

- 2017, doi: 10.1016/j.jaap.2017.11.001.
- [92] L. Shang, J. Ahrenfeldt, J. K. Holm, L. S. Bach, W. Stelte, and U. B. Henriksen, "Kinetic model for torrefaction of wood chips in a pilot-scale continuous reactor," *J. Anal. Appl. Pyrolysis*, vol. 108, pp. 109–116, 2014, doi: 10.1016/j.jaap.2014.05.010.
- [93] T. Khazraie Shoulaifar, N. Demartini, O. Karlström, and M. Hupa, "Impact of organically bonded potassium on torrefaction: Part 1. Experimental," *Fuel*, vol. 165, pp. 544–552, 2016, doi: 10.1016/j.fuel.2015.06.024.
- [94] T. Khazraie Shoulaifar, N. Demartini, O. Karlström, J. Hemming, and M. Hupa, "Impact of organically bonded alkali metals on torrefaction: Part 2. Modeling," *Fuel*, vol. 168, pp. 107–115, 2016, doi: 10.1016/j.fuel.2015.11.084.
- [95] A. Soria-Verdugo, E. Cano-Pleite, A. Panahi, and A. F. Ghoniem, "Kinetics mechanism of inert and oxidative torrefaction of biomass," *Energy Convers. Manag.*, vol. 267, no. June, p. 115892, 2022, doi: 10.1016/j.enconman.2022.115892.
- [96] L. G. O. B. S. C. Galvão, M. V. G. de Morais, A. T. do V. Vale, A. Caldeira-Pires, P. Rousset, and E. A. Silveira, "Combined thermo-acoustic upgrading of solid fuel: experimental and numerical investigation," in *28th European Biomass Conference and Exhibition*, 2020, pp. 6–9. doi: 10.5071/28thEUBCE2020-3DO.6.2.
- [97] M. Chai *et al.*, "Poplar wood torrefaction: Kinetics, thermochemistry and implications," *Renew. Sustain. Energy Rev.*, vol. 143, no. April 2020, 2021, doi: 10.1016/j.rser.2021.110962.
- [98] E. A. Silveira, S. M. Luz, R. M. Leão, P. Rousset, and A. Caldeira-Pires, "Numerical modeling and experimental assessment of sustainable woody biomass torrefaction via coupled TG-FTIR," *Biomass and Bioenergy*, vol. 146, no. April 2021, p. 105981, Mar. 2021, doi: 10.1016/j.biombioe.2021.105981.
- [99] W.-H. H. Chen, C. Fong Eng, Y.-Y. Y. Lin, Q.-V. V. Bach, V. Ashokkumar, and P.-L. L. Show, "Two-step thermodegradation kinetics of cellulose, hemicelluloses, and lignin under isothermal torrefaction analyzed by particle swarm optimization," *Energy Convers. Manag.*, vol. 238, no. January, p. 114116, Jun. 2021, doi: 10.1016/j.enconman.2021.114116.
- [100] E. A. Silveira *et al.*, "A potassium responsive numerical path to model catalytic torrefaction kinetics," *Energy*, vol. 239, p. 122208, Sep. 2022, doi: 10.1016/j.energy.2021.122208.

- [101] E. A. Silveira *et al.*, "Thermo-Acoustic Catalytic Effect on Oxidizing Woody Torrefaction," *Processes*, vol. 8, no. 11, p. 1361, Oct. 2020, doi: 10.3390/pr8111361.
- [102] E. A. Silveira *et al.*, "Heat treatment kinetics using three-stage approach for sustainable wood material production," *Ind. Crops Prod.*, vol. 124, pp. 563–571, 2018, doi: 10.1016/j.indcrop.2018.07.045.
- [103] B.-J. Lin *et al.*, "Modeling and prediction of devolatilization and elemental composition of wood during mild pyrolysis in a pilot-scale reactor," *Ind. Crops Prod.*, vol. 131, no. November 2018, pp. 357–370, May 2019, doi: 10.1016/j.indcrop.2019.01.065.
- [104] C. Branca and C. Di Blasi, "Kinetics of the isothermal degradation of wood in the temperature range 528–708 K," *J. Anal. Appl. Pyrolysis*, vol. 67, no. 2, pp. 207–219, May 2003, doi: 10.1016/S0165-2370(02)00062-1.
- [105] M. Safar *et al.*, "Catalytic effects of potassium on biomass pyrolysis, combustion and torrefaction," *Appl. Energy*, vol. 235, no. November 2018, pp. 346–355, 2019, doi: 10.1016/j.apenergy.2018.10.065.
- [106] C. Wang, X. Zhang, Y. Liu, and D. Che, "Pyrolysis and combustion characteristics of coals in oxyfuel combustion," *Appl. Energy*, vol. 97, pp. 264–273, Sep. 2012, doi: 10.1016/j.apenergy.2012.02.011.
- [107] C. Moon, Y. Sung, S. Ahn, T. Kim, G. Choi, and D. Kim, "Effect of blending ratio on combustion performance in blends of biomass and coals of different ranks," *Exp. Therm. Fluid Sci.*, vol. 47, pp. 232–240, May 2013, doi: 10.1016/j.expthermflusci.2013.01.019.
- [108] C. Wang, Y. Liu, X. Zhang, and D. Che, "A Study on Coal Properties and Combustion Characteristics of Blended Coals in Northwestern China," *Energy & Fuels*, vol. 25, no. 8, pp. 3634–3645, Aug. 2011, doi: 10.1021/ef200686d.
- [109] T. de P. Protásio, M. Guimarães Junior, S. Mirmehdi, P. F. Trugilho, A. Napoli, and K. M. Knovack, "COMBUSTION OF BIOMASS AND CHARCOAL MADE FROM BABASSU NUTSHELL," CERNE, vol. 23, no. 1, pp. 1–10, Mar. 2017, doi: 10.1590/01047760201723012202.
- [110] T. de P. Protásio, L. Bufalino, G. H. D. Tonoli, M. G. Guimarães Junior, P. F. Trugilho, and L. M. Mendes, "Brazilian lignocellulosic wastes for bioenergy production: Characterization and comparison with fossil fuels," *BioResources*, vol. 8, no. 1, pp. 1166–1185, 2013, doi: 10.15376/biores.8.1.1166-1185.

- [111] J. L. F. Alves et al., "Insights into the bioenergy potential of jackfruit wastes considering their physicochemical properties, bioenergy indicators, combustion behaviors, and emission characteristics," *Renew. Energy*, vol. 155, pp. 1328–1338, 2020, doi: 10.1016/j.renene.2020.04.025.
- [112] T. Oliveira and P. L. Albert, "Effects of torrefaction on energy properties of Eucalyptus grandis wood," *Cerne*, vol. 15, no. 4, pp. 446–452, 2009.
- [113] B. Arias, C. Pevida, J. Fermoso, M. G. Plaza, F. Rubiera, and J. J. Pis, "Influence of torrefaction on the grindability and reactivity of woody biomass," *Fuel Process. Technol.*, vol. 89, no. 2, pp. 169–175, 2008, doi: 10.1016/j.fuproc.2007.09.002.
- [114] A. F. Dias Júnior *et al.*, "Influência da adição de madeira de eucalipto à resíduos madeireiros urbanos frente à combustão," *Cerne*, vol. 23, no. 4, pp. 455–464, 2017, doi: 10.1590/01047760201723042337.
- [115] E. A. Silveira *et al.*, "Effect of torrefaction on thermal behavior and fuel properties of Eucalyptus grandis macro-particulates," *J. Therm. Anal. Calorim.*, vol. 138, no. 5, pp. 3645–3652, 2019, doi: 10.1007/s10973-018-07999-4.
- [116] M. C. Crisóstomo, M. F. da Silva, A. T. do Vale, and B. S. Chaves, "Caracterização Energética De Madeira De E. Grandis, Pinus Sp., T. Vulgaris E P. Lecointei," *Recur. Nat. Energ. Biomassa Florest.*, pp. 49–61, 2021, doi: 10.37885/210203270.
- [117] J. de O. Brotto *et al.*, "Investigation of the thermal behavior of Pinus wood pellets during torrefaction for application in metallurgical processes," *J. Mater. Res. Technol.*, vol. 19, pp. 3749–3759, 2022, doi: 10.1016/j.jmrt.2022.06.082.
- [118] L. E. Arteaga-Pérez, C. Segura, D. Espinoza, L. R. Radovic, and R. Jiménez, "Torrefaction of Pinus radiata and Eucalyptus globulus: A combined experimental and modeling approach to process synthesis," *Energy Sustain. Dev.*, vol. 29, pp. 13–23, 2015, doi: 10.1016/j.esd.2015.08.004.
- [119] M. Edo, V. Budarin, I. Aracil, P. Persson, and S. Jansson, "The combined effect of plastics and food waste accelerates the thermal decomposition of refuse-derived fuels and fuel blends," *Fuel*, vol. 180, pp. 424–432, 2016, doi: 10.1016/j.fuel.2016.04.062.
- [120] A. F. Dias Júnior et al., "Influence of Eucalyptus wood addition to urban wood waste during combustion," Cerne, vol. 23, no. 4, pp. 455–464, 2017, doi: 10.1590/01047760201723042337.
- [121] G. C. Lamas et al., "Effect of torrefaction on steam-enhanced co-gasification of an

- urban forest and landfill waste blend: H2 production and CO2 emissions mitigation," *Int. J. Hydrogen Energy*, 2023, doi: https://doi.org/10.1016/j.ijhydene.2023.03.367.
- [122] L. Dai *et al.*, "Integrated process of lignocellulosic biomass torrefaction and pyrolysis for upgrading bio-oil production: A state-of-the-art review," *Renew. Sustain. Energy Rev.*, vol. 107, no. January, pp. 20–36, 2019, doi: 10.1016/j.rser.2019.02.015.
- [123] S. W. Du, W. H. Chen, and J. A. Lucas, "Pretreatment of biomass by torrefaction and carbonization for coal blend used in pulverized coal injection," *Bioresour. Technol.*, vol. 161, pp. 333–339, 2014, doi: 10.1016/j.biortech.2014.03.090.
- [124] J. A. N. BATISTA, "Torrefação do Pinus elliottii para fins energéticos," Unessp, 2015.
- [125] N. Schmitt, A. Apfelbacher, N. Jäger, R. Daschner, F. Stenzel, and A. Hornung, "Thermo-chemical conversion of biomass and upgrading to biofuel: The Thermo-Catalytic Reforming process – A review," *Biofuels, Bioprod. Biorefining*, vol. 13, no. 3, pp. 822–837, 2019, doi: 10.1002/bbb.1980.
- [126] L. Shang *et al.*, "Intrinsic kinetics and devolatilization of wheat straw during torrefaction," *J. Anal. Appl. Pyrolysis*, vol. 100, pp. 145–152, 2013, doi: 10.1016/j.jaap.2012.12.010.
- [127] P. Kitrungloadjanaporn, L. Q. Sang, J. Pukdum, and T. Phengpom, "Evaluating the role of operating temperature and residence time in the torrefaction of betel nutshells for solid fuel production," *Int. J. Renew. Energy Dev.*, vol. 12, no. 6, pp. 1113–1122, 2023, doi: 10.14710/ijred.2023.58228.
- [128] M. Phanphanich and S. Mani, "Impact of torrefaction on the grindability and fuel characteristics of forest biomass," *Bioresour. Technol.*, vol. 102, no. 2, pp. 1246–1253, 2011, doi: 10.1016/j.biortech.2010.08.028.
- [129] J. C. G. da Silva, S. L. F. Andersen, R. L. Costa, R. de F. P. M. Moreira, and H. J. José, "Bioenergetic potential of Ponkan peel waste (Citrus reticulata) pyrolysis by kinetic modelling and product characterization," *Biomass and Bioenergy*, vol. 131, p. 105401, Dec. 2019, doi: 10.1016/j.biombioe.2019.105401.
- [130] S. Munir, S. S. Daood, W. Nimmo, A. M. Cunliffe, and B. M. Gibbs, "Thermal analysis and devolatilization kinetics of cotton stalk, sugar cane bagasse and shea meal under nitrogen and air atmospheres," *Bioresour. Technol.*, vol. 100, no. 3, pp. 1413–1418, Feb. 2009, doi: 10.1016/j.biortech.2008.07.065.
- [131] J. Xing, K. Luo, H. Wang, and J. Fan, "Estimating biomass major chemical

- constituents from ultimate analysis using a random forest model," *Bioresour. Technol.*, vol. 288, p. 121541, Sep. 2019, doi: 10.1016/j.biortech.2019.121541.
- [132] T. de P. Protásio *et al.*, "Insights in quantitative indexes for better grouping and classification of Eucalyptus clones used in combustion and energy cogeneration processes in Brazil," *Biomass and Bioenergy*, vol. 143, no. October, p. 105835, Dec. 2020, doi: 10.1016/j.biombioe.2020.105835.
- [133] N. B. Park, S. Y. Park, J. J. Kim, D. G. Choi, B. Y. Yun, and J. C. Hong, "Technical and economic potential of highly efficient boiler technologies in the Korean industrial sector," *Energy*, vol. 121, pp. 884–891, 2017, doi: 10.1016/j.energy.2017.01.022.
- [134] K. Candelier, M.-F. Thevenon, A. Petrissans, S. Dumarcay, P. Gerardin, and M. Petrissans, "Control of wood thermal treatment and its effects on decay resistance: a review," *Ann. For. Sci.*, vol. 73, no. 3, pp. 571–583, Sep. 2016, doi: 10.1007/s13595-016-0541-x.
- [135] J. de Oliveira Brotto *et al.*, "Mechanistic insights and kinetics of torrefaction of pine wood biomasses using solid-state NMR," *J. Anal. Appl. Pyrolysis*, vol. 172, no. February, p. 106019, Jun. 2023, doi: 10.1016/j.jaap.2023.106019.
- [136] E. A. Silveira, L. A. Macedo, K. Candelier, P. Rousset, and J.-M. Commandré, "Assessment of catalytic torrefaction promoted by biomass potassium impregnation through performance indexes," *Fuel*, vol. 304, no. February, p. 121353, Nov. 2021, doi: 10.1016/j.fuel.2021.121353.
- [137] W. H. Chen, M. Y. Huang, J. S. Chang, and C. Y. Chen, "Thermal decomposition dynamics and severity of microalgae residues in torrefaction," *Bioresour. Technol.*, vol. 169, pp. 258–264, 2014, doi: 10.1016/j.biortech.2014.06.086.
- [138] M. González Martínez *et al.*, "Torrefaction of cellulose, hemicelluloses and lignin extracted from woody and agricultural biomass in TGA-GC/MS: Linking production profiles of volatile species to biomass type and macromolecular composition," *Ind. Crops Prod.*, vol. 176, no. December 2021, p. 114350, Feb. 2022, doi: 10.1016/j.indcrop.2021.114350.
- [139] E. Peduzzi, G. Boissonnet, G. Haarlemmer, C. Dupont, and F. Maréchal, "Torrefaction modelling for lignocellulosic biomass conversion processes," *Energy*, vol. 70, pp. 58– 67, 2014, doi: 10.1016/j.energy.2014.03.086.
- [140] T. de P. Protásio et al., "Assessing Proximate Composition, Extractive Concentration,

- and Lignin Quality to Determine Appropriate Parameters for Selection of Superior Eucalyptus Firewood," *BioEnergy Res.*, vol. 12, no. 3, pp. 626–641, Sep. 2019, doi: 10.1007/s12155-019-10004-x.
- [141] J. J. Lu and W. H. Chen, "Investigation on the ignition and burnout temperatures of bamboo and sugarcane bagasse by thermogravimetric analysis," *Appl. Energy*, vol. 160, no. 2015, pp. 49–57, 2015, doi: 10.1016/j.apenergy.2015.09.026.
- [142] A. Magdziarz, M. Wilk, and R. Straka, "Combustion process of torrefied wood biomass: A kinetic study," *J. Therm. Anal. Calorim.*, vol. 127, no. 2, pp. 1339–1349, 2017, doi: 10.1007/s10973-016-5731-0.
- [143] M. Safar *et al.*, "Effects of impregnated potassium on biomass torrefaction," *Energy Procedia*, vol. 158, pp. 55–60, 2019, doi: 10.1016/j.egypro.2019.01.035.
- [144] L. G. Fraga, S. Teixeira, and D. Soares, "Behavior and Kinetics of Pine Wood Particles Using," *Energies*, vol. 13, no. 2756, pp. 1–22, 2020.
- [145] M. Mureddu, F. Dessì, A. Orsini, F. Ferrara, and A. Pettinau, "Air- and oxygen-blown characterization of coal and biomass by thermogravimetric analysis," *Fuel*, vol. 212, no. April 2017, pp. 626–637, 2018, doi: 10.1016/j.fuel.2017.10.005.
- [146] E. A. Silveira *et al.*, "A hybrid optimization approach towards energy recovery from torrefied waste blends," *Renew. Energy*, May 2023, doi: 10.1016/j.renene.2023.05.053.
- [147] B. H. Lee, L. Sh, D. G. Lee, and C. H. Jeon, "Effect of torrefaction and ashless process on combustion and NOx emission behaviors of woody and herbaceous biomass," *Biomass and Bioenergy*, vol. 151, no. April, p. 106133, 2021, doi: 10.1016/j.biombioe.2021.106133.
- [148] IEA, "Key World Energy Statistics 2021 Statistics Report," IEA Publ., pp. 1–82, 2021.
- [149] J. Roy, P. Sarkar, S. Biswas, and A. Choudhury, "Predictive equations for CO2 emission factors for coal combustion, their applicability in a thermal power plant and subsequent assessment of uncertainty in CO2 estimation," *Fuel*, vol. 88, no. 5, pp. 792–798, 2009, doi: 10.1016/j.fuel.2008.11.023.
- [150] Í. M. L. Mendes, M. S. B. Fialho, R. M. Leão, E. A. Silveira, and S. M. da Luz, "Processing Biodegradable Blends of Hemicellulose with Polyhydroxybutyrate and Poly (Lactic Acid)," *Mater. Res.*, vol. 26, no. e20220390, 2023, doi: 10.1590/1980-5373-mr-2022-0390.

[151] G. F. Ghesti, E. A. Silveira, M. G. Guimarães, R. B. W. W. Evaristo, and M. Costa, "Towards a sustainable waste-to-energy pathway to pequi biomass residues: Biochar, syngas, and biodiesel analysis," *Waste Manag.*, vol. 143, no. November 2021, pp. 144–156, Apr. 2022, doi: 10.1016/j.wasman.2022.02.022.